Geochimica et Cosmochimica Acta Vol. 51, pp. 1685–1704

0016-7037/87/$3.00 + .00

Alteration of Al-rich inclusions inside amoeboid olivine aggregates in the Allende meteorite

AKIHIKO HASHIMOTO[1] and LAWRENCE GROSSMAN[2]
Department of the Geophysical Sciences, The University of Chicago, 5734 South Ellis Avenue, Chicago, IL 60637, U.S.A.

(*Received November* 28,1986; *accepted in revised form March* 23, 1987)

Abstract—Lightly altered Al-rich inclusions in amoeboid olivine aggregates have cores containing primary melilite + fassaite + spinel + perovskite and no secondary alteration products. In moderately altered inclusions, whose cores now contain only fassaite + spinel + perovskite, melilite was replaced by a fine-grained mixture of grossular + anorthite + feldspathoids and perovskite was partially replaced by ilmenite. In heavily altered inclusions, fassaite has been replaced by a mixture of phyllosilicates + ilmenite and the remaining primary phases are spinel ± perovskite. In very heavily altered inclusions, no primary phases remain, the spinel having reacted to form either phyllosilicates or a mixture of olivine + feldspathoids. This sequence of alteration reactions may reflect successively lower solar nebular equilibration temperatures. During alteration, SiO_2, Na_2O, K_2O, FeO, Cr_2O_3, H_2O and Cl were introduced into the inclusions and CaO was lost. MgO may have been lost during the melilite reaction and added during formation of phyllosilicates. Electron microprobe analyses indicate that the phyllosilicates are a mixture of Na-rich phlogopite and chlorite or Al-rich serpentine. Thermodynamic calculations suggest that, at a solar nebular water fugacity of 10^{-6}, Na-rich phlogopite could have formed from fassaite at ~470 K and chlorite from Na-rich phlogopite at ~328 K. Olivine mantling Al-rich inclusions is not serpentinized, suggesting that these objects stopped equilibrating with the nebular gas above 274 K.

INTRODUCTION

AMOEBOID OLIVINE AGGREGATES are greyish-brown, irregularly-shaped objects composed predominantly of subspherical lumps (100–1000 μm in diameter) of polygonal olivine crystals (1–20 μm in size). In the first petrographic study of these aggregates, GROSSMAN and STEELE (1976) found assemblages of spinel, perovskite, Ca-rich pyroxene and feldspathoids within the olivine lumps. The latter assemblages, as well as the loosely-packed, angular, subrounded or euhedral olivine crystals making up the interstitial matrix material between the lumps, were first seen clearly in the scanning electron microscope (SEM) study of BAR-MATTHEWS *et al.* (1979). GROSSMAN and STEELE (1976) and GROSSMAN *et al.* (1979) proposed that the olivine lumps formed by solar nebular condensation of olivine at ~1400 K around pre-existing high-temperature condensate assemblages containing spinel and perovskite and that the presence of alteration products such as feldspathoids in the latter assemblages implies that interaction between grains and gas continued in the temperature range 500–900 K. In a trace element study of amoeboid olivine aggregates, GROSSMAN *et al.* (1979) found that refractory elements are uniformly enriched relative to Cl chondrites but by a lower factor than in Allende coarse-grained inclusions. This was attributed to dilution of high-temperature condensate assemblages similar to those of coarse-grained inclusions by olivine which is relatively free of refractory elements. KORNACKI and WOOD (1984b) also suggested that amoeboid olivine aggregates, "Type 1B inclusions" in their study, are assemblages of nebular condensates.

The Al-rich inclusions of this study are spherically- to irregularly-shaped, 5–300 μm-sized, rimmed objects. They are the same as the "high-temperature condensate assemblages" of our earlier work on Allende amoeboid olivine aggregates and the "concentric objects" or "spinel-rich nodules" observed by later SEM studies in Type 1B inclusions in Allende (KORNACKI and FEGLEY, 1984; KORNACKI and WOOD, 1984a, 1985) and in Ca-, Al-rich inclusions in Mokoia (COHEN *et al.*, 1983) and Kaba (FEGLEY and POST, 1985). In contrast to the previous studies, the present work is concerned with the sequence of alteration processes that affected the Al-rich inclusions. Preliminary reports of our findings were given by HASHIMOTO and GROSSMAN (1984) and GROSSMAN *et al.* (1986).

PROCEDURES

Samples

Nine amoeboid olivine aggregates were studied in seven polished thin sections of the Allende meteorite. Petrographic descriptions of two of these objects, TS11F1 (*Thin Section #11, Feature #1*) and TS43F1, have already been published by GROSSMAN and STEELE (1976) and BAR-MATTHEWS *et al.* (1979). In addition, trace element data have been presented by GROSSMAN *et al.* (1979) and EKAMBARAM *et al.* (1985) for splits of four of the samples studied herein, TS43F1, TS51F1, TS55F1 and TS58F1, obtained by excavation from the mirror images of the inclusions in thin section on facing slabs of the meteorite. Sample numbers for Al-rich inclusions in amoeboid olivine aggregates are derived as in 55101 (*TS55F1 #01*).

Analytical techniques

All samples were examined with a JEOL JSM-35 SEM equipped with a back-scattered electron (BSE) detector and a Si(Li) X-ray analyzer. Mineral analyses were obtained at 15

[1] *Present address:* Smithsonian Astrophysical Observatory, 60 Garden St., Cambridge, MA 02138, U.S.A.

[2] Also at the Enrico Fermi Institute, The University of Chicago.

keV and 0.15 nA using the latter device, an on-line PDP 11/03 computer and a program based on the procedure of BENCE and ALBEE (1968). Analytical volumes were ~1 μm^3. Natural and synthetic minerals and glasses of known compositions were used for standards. For these energy-dispersive analyses, 2σ uncertainties due to counting statistics are approximately ±0.2 wt% for concentrations of all elements above 1 wt% and ±0.1 wt% for concentrations below 1 wt%.

Wavelength-dispersive, twelve-element mineral analyses were obtained for four amoeboid olivine aggregates with a JXA-733 automated electron microprobe (EPMA), operated at 15 keV and a spot diameter of ~3 μm. Three beam currents were used: 30 nA for alkali-free minerals and 3 or 1 nA for nepheline and alkali-rich, ragged material. Sodium evaporation from polycrystalline nepheline was noted even at these low beam currents. To eliminate this problem, the SEM was used for determination of Na_2O and K_2O in such nepheline. Because of possible uncertainties due to background subtraction for Na_2O and to low concentrations for K_2O, however, these SEM data were corrected by means of calibration curves between SEM and EPMA data obtained from single nepheline crystals for which no alkali evaporation was detected in EPMA analyses. Vanadium analyses were corrected for Ti$K\beta$ interference by subtracting .0042 × wt% TiO_2 from the raw V_2O_3 contents. This correction factor was derived from a V-free ilmenite standard. For all elements except Ti, 2σ uncertainties due to counting statistics are ±0.04 wt% for concentrations above 2 wt% and ± 0.02 wt% for lower concentrations. For Ti, uncertainties are ±0.10 wt% above 2 wt% and ±0.05 wt% for lower concentrations.

TEXTURE AND MINERALOGY

Al-rich inclusions

We performed a detailed SEM and EPMA study of nearly fifty Al-rich inclusions in three amoeboid olivine aggregates and a more cursory survey of more than a hundred Al-rich inclusions in five others. It seems appropriate to classify these inclusions on the basis of their core mineralogy. The first group have cores of melilite, Ti-rich fassaite and spinel with minor perovskite. The second group have cores of fassaite, spinel and a relatively fine-grained mixture of anorthite, grossular and feldspathoids, with minor perovskite and/or ilmenite. The third group have cores of spinel and a fine-grained mixture of phyllosilicates and feldspathoids with minor ilmenite. The final group have cores containing only the fine-grained material typical of that in the third group. As will be shown, the fine-grained materials are replacing the primary phases, and the essential difference between these four groups is the mineralogical composition of the remaining primary phases: melilite + fassaite + spinel + perovskite in the first group, fassaite + spinel ± perovskite in the second, spinel ± perovskite in the third and none in the fourth. HASHIMOTO and GROSSMAN (1984) suggested that these inclusions exhibit a range of alteration intensity and that inclusion cores were composed originally of melilite, fassaite, spinel and perovskite. Therefore, we label the above four groups of Al-rich inclusions lightly altered, moderately altered, heavily altered and very heavily altered, respectively.

The lightly altered type is rare. Only two have been found so far, in one amoeboid olivine aggregate, TS55F1. Moderately, heavily and very heavily altered types occur in many amoeboid aggregates. There is a general tendency for the size of Al-rich inclusions to decrease with increasing alteration intensity. The two lightly altered inclusions are approximately 300 μm in diameter. Moderately and heavily altered types are typically 50–150 μm and very heavily altered types <5–50 μm in their longest dimensions.

Lightly altered type. 55101 is a near-spherical inclusion (Fig. 1), 270 μm in diameter, composed of four concentric zones. The core, 100 μm in diameter, consists mostly of melilite (Ge 85–96) enclosing skeletal spinel crystals (<20 μm in length).

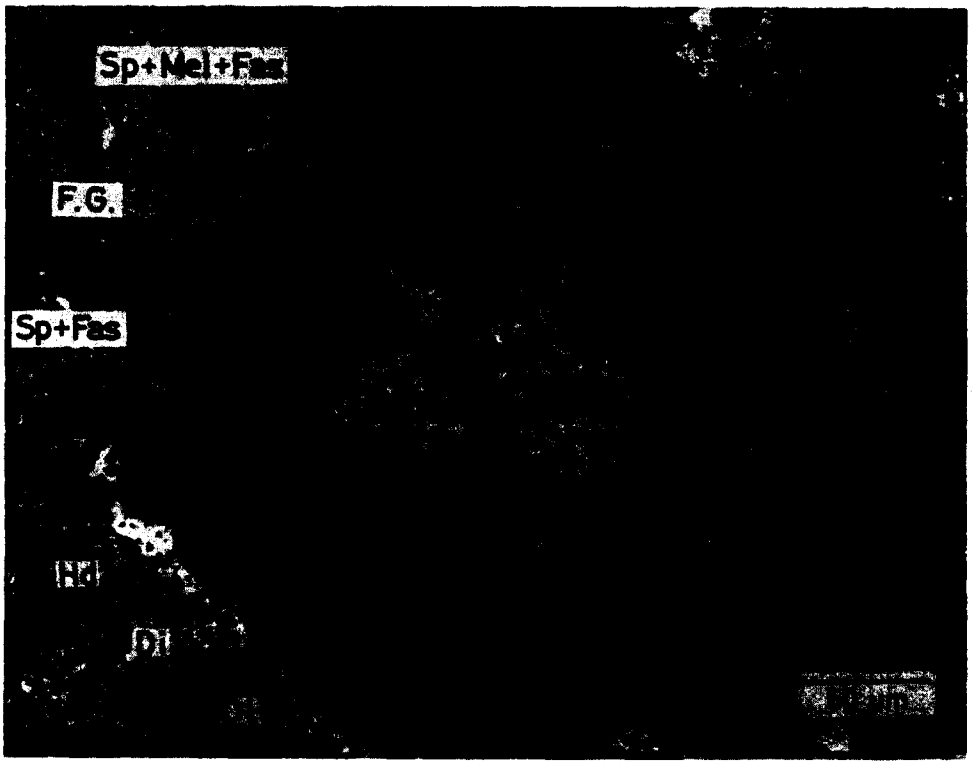

FIG. 1. Back-scattered electron (BSE) image of 55101, a lightly altered inclusion, showing cavity-free core consisting of skeletal spinel (Sp; dark) in melilite (Mel; light), fine-grained (F.G.) inner mantle, cavity-poor outer mantle made mostly of spinel and fassaite (Fas) and pyroxene rim grading outward from fassaite to aluminous diopside (Di) in composition. Entire inclusion is enclosed by olivine (Ol), followed by a discontinuous, hedenbergite (Hd)-rich rind.

Minor Ti-rich fassaite occurs in pockets between spinel crystals or abutting against the longest sides of spinel crystals. Rare perovskite occurs within or abutting against spinel. Voids are rare and small. Enclosing the core is an ~40 μm thick inner mantle (Fig. 2) composed of skeletal spinel crystals decorated with Ti-rich fassaite, and of a cavity-riddled mixture of feldspathoids (mostly nepheline), anorthite and grossular. In the outer mantle (Fig. 3), spinel is more rounded, fassaite more abundant and feldspathoids, anorthite and grossular much less abundant than in the inner mantle. Ilmenite occurs as tiny blebs (≤1 μm). Fassaite is texturally continuous in some places with fassaite in the outermost zone, the rim. In other places, cavities separate fassaite in the outer mantle from that in the rim. These are partially filled with nepheline or a ragged material rich in Mg, Al and Si with a much larger K/Na ratio than nepheline. It is a mixture of phyllosilicates (see Mineral Chemistry). Such material also often occurs without nepheline between spinel grains in the outer part of the mantle (Fig. 3). Frequently, very fine-grained ilmenite is smeared throughout this material.

The rim is a 5μm thick band grading inward from aluminous diopside to fassaite which is poorer in Al and Ti than that in the interior. The rim contains many small cavities but is less porous than the mantle. Enclosing the rim is a porous, 0–50 μm thick olivine crust, followed by a discontinuous, 5 μm thick rind made mostly of hedenbergite and salite with occasional olivine and nepheline, hereinafter called "the hedenbergite-rich assemblage". The olivine crust consists of 5–20 μm-sized, polygonal olivine grains which are zoned from Fo 95 outward to Fo 85. In places, the hedenbergite-rich rind is in direct contact with the clinopyroxene rim. We define the boundary of each Al-rich inclusion at the outer surface of the clinopyroxene rim. A single olivine lump often contains many Al-rich inclusions.

55102 is an oval-shaped, 300 × 200 μm inclusion (Fig. 4). Its core consists mostly of spinel which encloses wormy melilite (Ge 92–98), Ti-rich fassaite and minor perovskite. Melilite, in turn, encloses small (1–2 μm) spinel grains. Fassaite occurs preferentially in pockets between spinel grains. Cavities are rare, partially filled with nepheline, anorthite and grossular and tend to be contiguous with melilite. Surrounding the core is an ~20 μm thick mantle consisting of a cavity-riddled, fine-grained mixture of anorthite, nepheline, iron-rich spinel, and minor grossular and ilmenite, which also embays and veins the core along channels in melilite (Figs. 4, 5). Outside the mantle is a 3 μm thick, inner rim of Ti-rich fassaite and an ~15 μm thick outer rim of aluminous diopside. In places, ilmenite-laden, ragged phyllosilicates are intergrown with and partially replace fassaite in the inner rim layer (Fig. 6). Enclosing the inclusion is a cluster of zoned, polygonal olivine grains with an occasional, thin rind of the hedenbergite-rich assemblage.

Studies of alteration products in coarse-grained inclusions (ALLEN *et al.*, 1978; WARK, 1981; MACPHERSON *et al.*, 1981) show that, of all primary phases, melilite is the most susceptible to secondary alteration which converts it to anorthite, grossular and feldspathoids. These are precisely the minerals seen in the mantles of 55101 and 55102, which differ from their cores by the absence of melilite. In 55101, skeletal spinel crystals often protrude from the core into the mantle (Fig. 2) and Ti-rich fassaite abuts against spinel both in the core and in the mantle (Fig. 2), indicating textural continuity between the two zones. The only difference in mineralogy and texture be-

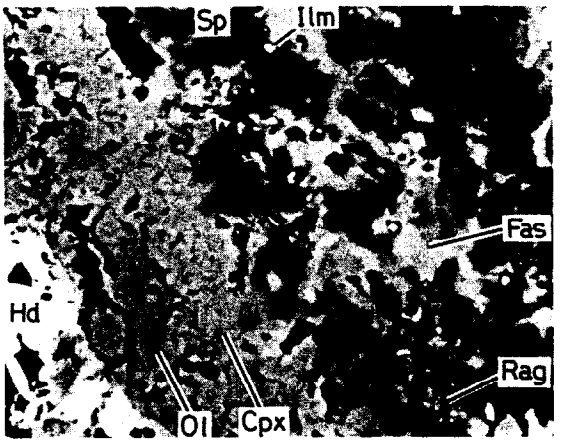

FIG. 3. BSE image of the outer mantle of 55101, showing interlocking spinel and fassaite. Fassaite is contiguous with rim clinopyroxene (Cpx) in places. Ragged phyllosilicate (Rag) fills some of the spaces between spinel grains. In this area, the olivine crust is very thin and is coated by a hedenbergite-rich rind. Width of field is 60 μm. Ilm—ilmenite. Other abbreviations as used previously.

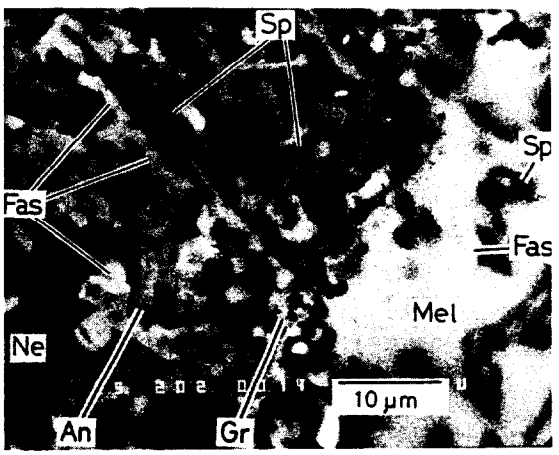

FIG. 2. BSE image of core (right)-mantle (left) boundary of 55101, showing spinel crystals of similar morphology and adjoining fassaite in both areas. In the mantle, interstices between spinel grains are partially filled with nepheline (Ne), anorthite (An) and minor grossular (Gr). Other abbreviations as used previously.

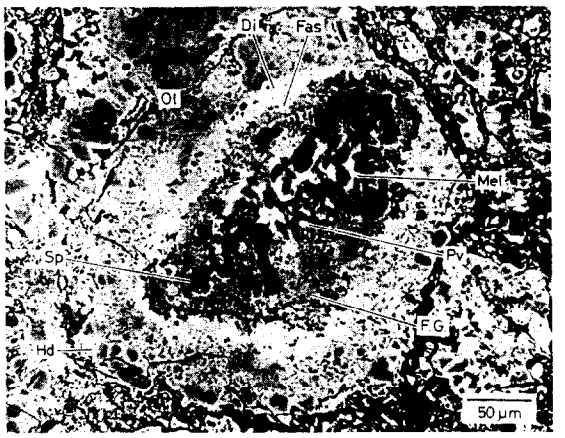

FIG. 4. BSE image of 55102, a lightly altered inclusion, showing a core of wormy melilite and spinel, and a fine-grained mantle of iron-rich spinel and alteration minerals which embays and veins the core along melilite channels. Entire inclusion is surrounded by a massive, polycrystalline crust of zoned, polygonal olivine grains. Pv–perovskite. Other abbreviations as used previously.

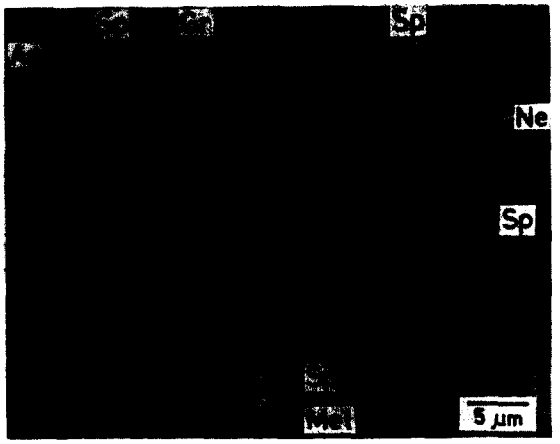

FIG. 5. BSE image of the core (bottom and sides)-mantle (top) boundary of 55102. Small spinel grains occur within both core melilite and fine-grained mantle material consisting mostly of anorthite, feldspathoids and grossular. Mantle spinel is richer in FeO. Abbreviations as used previously.

tween core and mantle of lightly altered inclusions is that a fine-grained, porous mixture of anorthite, grossular and feldspathoids occupies the same textural position in the mantle as melilite does in the core. These observations strongly suggest that melilite was altered in the outer parts of these inclusions but remained intact in the interiors. Fassaite and spinel are interpreted to have survived even in the mantles of these inclusions because of their relatively high resistance to alteration under the conditions of melilite alteration.

Moderately altered type. The only primary phases remaining in the cores of Al-rich inclusions of this type are spinel, fassaite and, in some cases, perovskite. The remarkable similarity in mineralogy and texture between the cores of inclusions belonging to this type, such as 55108, and the mantles of lightly altered inclusions like 55101 can be seen clearly in Fig. 7. In the cores of moderately altered inclusions, anorthite is enclosed by irregular patches of nepheline and sodalite, a texture frequently observed in lightly altered inclusions and indicating that feldspathoids form by reaction of anorthite. An example of a particularly spinel-rich variety of this type of inclusion, 51101, is shown in Fig. 8. In such inclusions, spinel is so much more abundant than fassaite that the former encloses the latter, while in the spinel-poor variety, such as 55108, fassaite decorates spinel. Figure 8 shows that the ragged material is sometimes found partially replacing fassaite in the inner rim and outer core. Ilmenite is more abundant than perovskite in moderately altered inclusions. Cavities in their cores, empty or partially filled with grossular and nepheline, are frequently lined by fassaite, either partially or completely.

55106 (Fig. 9) is a cluster of nearly twenty, 50–150 μm-sized, Al-rich inclusions, most of which belong to the spinel-rich variety of the moderately altered type and some to the heavily altered type. As seen in Fig. 9, the cores of some inclusions are spinel nodules while the cores of others are spinel bands. Both types of cores are rimmed by clinopyroxene. The olivine crust which usually surrounds Al-rich inclusions is thin or absent in many places in 55106, occasionally placing individually distinguishable Al-rich inclusions in direct contact with one another with no intervening olivine. Others may be connected in the third dimension. Sometimes, irregularly-shaped islands of unzoned, Fe-poor olivine (Fo 98) are found inside a clinopyroxene zone sandwiched between spinel zones. These islands are probably fingers of the olivine mantle which intrude into deep pockets between individual Al-rich inclusions or between segments of a single, highly irregular one. Clusters of inclusions such as 55106 are found in many amoeboid olivine aggregates. The Al-rich inclusions comprising 55106 are very similar in mineralogy and texture to spinel-pyroxene inclusions described by MACPHERSON *et al.* (1983) in the C2 chondrite Murchison.

Heavily altered type. In this type of Al-rich inclusion, spinel and, rarely, perovskite are the only primary minerals. 55115 (Fig. 10) is a rounded, 80 μm-sized inclusion with a spinel core. The spinel is cavity-riddled and irregularly veined and embayed by ragged material similar to that found just inside the rim of lightly and moderately altered inclusions. Fassaite is rare, as its absence defines the heavily altered type. When it occurs, it is attached to spinel. Ilmenite occurs as <1–3 μm-sized grains enclosed by the ragged material, and is probably also the phase that exists as a swarm of fine particles dispersed in and looking like an overprinted smear onto the ragged material. The ragged material is porous and frequently has the appearance of a bundled hay stack in which sub-parallel strands are 0.1–0.3 μm thick and 1–2 μm long. Around the core is a 5 μm thick zone of ragged material which contains ilmenite only of the fine-grained type. Outside of this zone is an unusually thin rim composed only of aluminous diopside, as if the inner fassaite rim found on lightly and moderately altered inclusions has been replaced by ragged material in this heavily altered inclusion. In places, ragged material is in direct contact with olivine. The fine-grained ilmenite may also be an alteration product of fassaite while the coarser ilmenite may have been derived from perovskite. Replacement of fassaite by a ragged-looking phyllosilicate was reported previously by DOMINIK *et al.* (1978) in a fassaite-, forsterite-, spinel-rich Allende inclusion.

Some inclusions in the cluster 55106 are of the heavily altered type (Fig. 9). As in 55115, ragged material with ilmenite spots is sandwiched between the spinel-rich cores and the thin, aluminous diopside rims of these inclusions, and also embays and veins the cores. Comparison of these inclusions with the moderately altered members of 55106 shows that the total thickness of the band of ragged material and the aluminous diopside rim is approximately equal to the total thickness of the clinopyroxene rim in the latter inclusions (~10 μm). This fact again suggests replacement of fassaite by the ragged material.

As in the case of moderately altered inclusions, there are both spinel-rich and spinel-poor members of the heavily altered type, the latter being characterized by a higher proportion of melilite alteration products to spinel than the former. In heavily altered, spinel-poor inclusions, nepheline shows similar textural relationships with spinel and clinopyroxene to those in 55107 and 55108, the moderately altered, spinel-poor inclusions, but the other melilite alteration products, anorthite and grossular, are missing from heavily altered ones, possibly

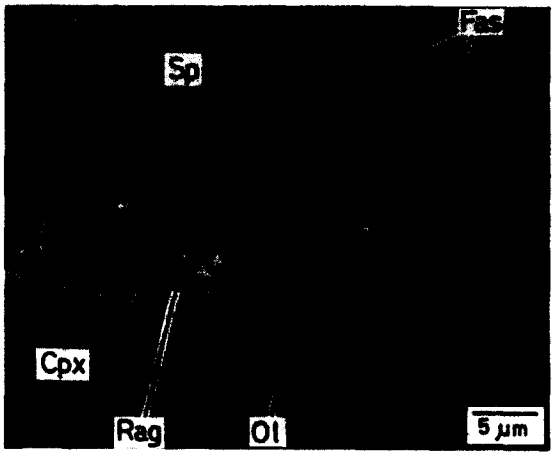

FIG. 6. BSE image of 55102, showing fine-grained interior (top) and clinopyroxene rim (bottom) which has been partially replaced by fine-grained ragged material containing fine ilmenite grains. Abbreviations as used previously.

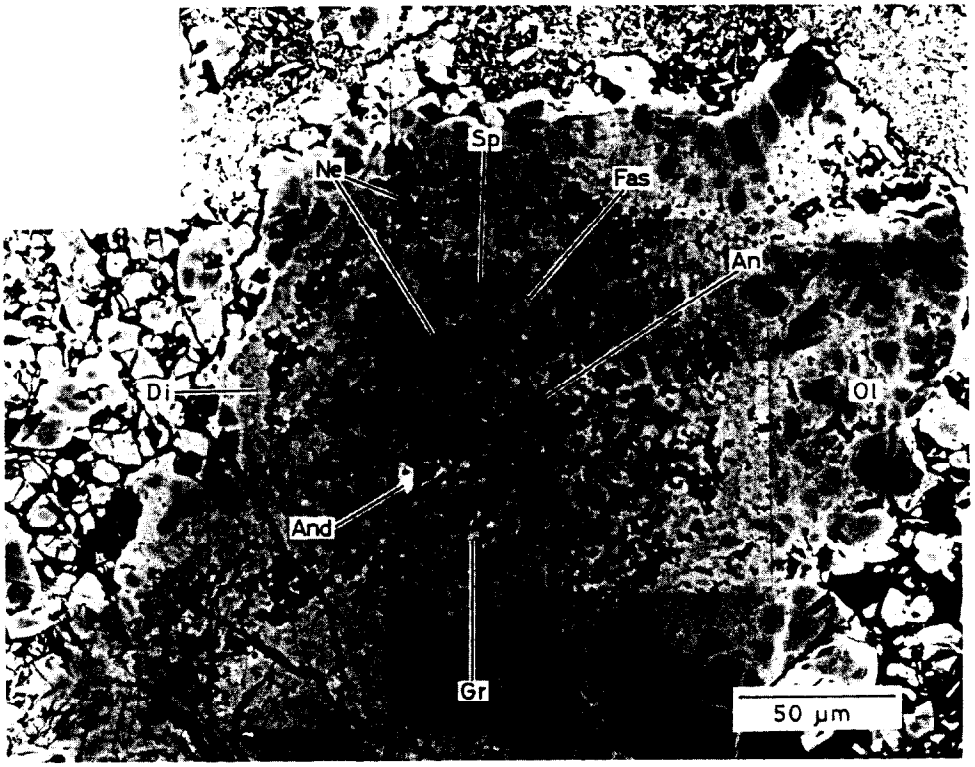

FIG. 7. BSE image of 55108, a moderately altered inclusion. In the core of this inclusion, like the mantle of 55101 (Fig. 2), elongated spinel grains decorated with fassaite are separated by cavities and interstitial anorthite, feldspathoids, minor grossular and rare andradite (And). Near the pyroxene rim, fassaite is intergrown with spinel and contiguous with rim pyroxene in places. Note the thick olivine crust around this inclusion and the euhedral shapes of the matrix olivine grains outside of the inclusion to the upper right. Other abbreviations as used previously.

due to their greater degree of alteration. In heavily altered, spinel-poor inclusions, the ragged material surrounds irregularly-shaped spinel and clinopyroxene grains. Most of the

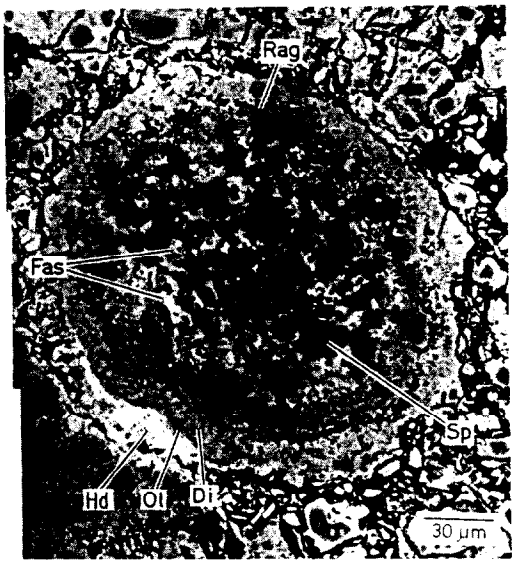

FIG. 8. BSE image of 51101, a moderately altered, spinel-rich inclusion, showing abundant cavities associated with fassaite in its core. Bright specks are perovskite and ilmenite. Note the void-rich, ragged phyllosilicate at the contact between the core and clinopyroxene rim. Abbreviations as used previously.

clinopyroxene is Al-diopside rather than fassaite, again suggesting selective replacement of fassaite by the ragged material.

Very heavily altered type. Members of this type of Al-rich inclusion contain no melilite or fassaite and less than 10% spinel by volume in their cores. Figure 11 shows an example, inclusion 55111. Spinel is embedded in a cavity-riddled matrix made mostly of the ragged material. Edges of spinel grains are highly irregular and embayed by the latter material, as are rare, Ti-, Al-poor fassaite grains. Massive and fine particles of ilmenite are dispersed in the ragged material. Fine-grained olivine is sometimes found attached to spinel. The core is separated from a surrounding, 5 μm thick, aluminous diopside rim by cavities. The Ti-, Al-rich clinopyroxene layer is missing, as in heavily altered inclusions. In another example, a cavity-riddled core made mostly of ragged material is crossed by a bridge of diopside which is connected at both ends to the inner wall of a diopside rim, again illustrating the relative resistance of diopside to alteration.

Another type of very heavily altered inclusion consists mostly of olivine enclosed by feldspathoids, although relatively large (≥20 μm) members of this group also have discontinuous aluminous diopside rims. Frequently, feldspathoids also enclose spinel and clinopyroxene grains attached to olivine. Nepheline is more abundant than sodalite. As the proportion of olivine to spinel and clinopyroxene increases, olivine crystal faces become more well-developed (Fig. 12) and the aluminous diopside rims become thinner and discontinuous. As also seen in Fig. 12, this type of inclusion can coexist in the same olivine clump with small, moderately altered inclusions having spinel + feldspathoids ± clinopyroxene cores and diopside rims. A continuous variation observed between these two inclusion types suggests replacement of spinel and pyroxene by olivine and feldspathoids.

Small (<5 μm), monomineralic nepheline inclusions are distributed throughout the olivine clumps, usually at olivine

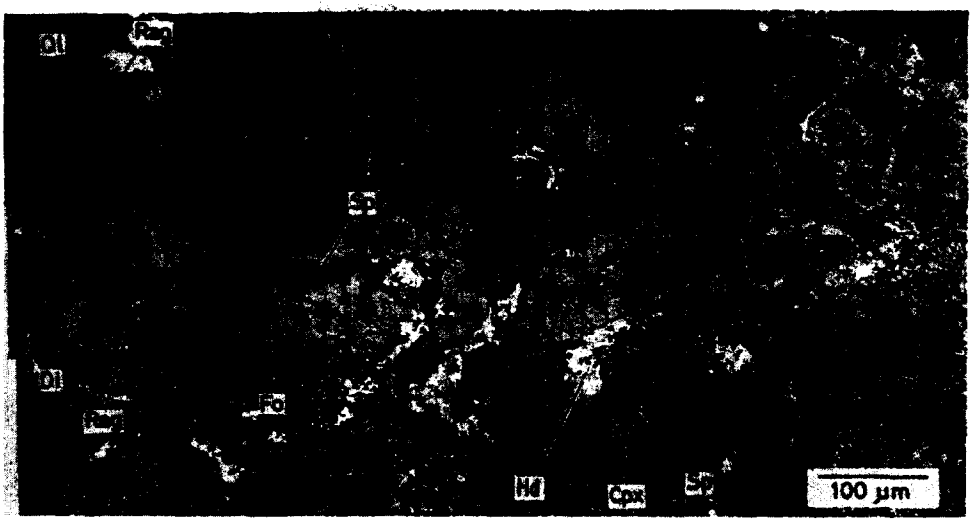

FIG. 9. BSE image of 55106, a cluster of moderately and heavily altered, spinel-rich inclusions which are frequently in direct contact with one another. Rims of clinopyroxene, grading outward from fassaite to diopside, enclose cores of nodular or banded spinel in the middle of the cluster. Three inclusions on the far left have spinel-rich cores enclosed by ilmenite (bright)-laden, ragged material which is enclosed by diopside. The ragged material embays and veins the core in one of these. Occasionally, forsteritic olivine (Fo) is enclosed within pyroxene rims. Other abbreviations as used previously.

grain boundaries and sometimes with specks of aluminous diopside attached to the inner wall of the surrounding olivine. These may be very heavily altered inclusions in which secondary olivine simply became intergrown with olivine in the surrounding clumps and in which even the aluminous diopside rims were altered to olivine and nepheline.

Hedenbergite-rich assemblage

Hedenbergite is the predominant phase in this assemblage. Andradite is rare. The remaining phases are enclosed within hedenbergite as small (<20 μm), irregular patches. Salitic pyroxene (En 45–38 Fs 3–9 Wo 53–47 with 1–3% Al_2O_3) is the second most abundant phase in most places but is more abundant than hedenbergite where the assemblage fills cavities. In those cases, hedenbergite tends to line cavity walls and salite fills the centers. An intergrowth of unzoned olivine (Fo ~ 90) with less abundant nepheline is often enclosed by hedenbergite. Occasionally, accessory metal ($\sim Ni_{66}Fe_{34}$) and pentlandite are found within salitic pyroxene and olivine. An important feature common to all occurrences of this assemblage is that it shows sharp boundaries against olivine (Fig. 11). Although it decorates outer surfaces of olivine clumps and lines cavities within them, it is never intergrown with olivine.

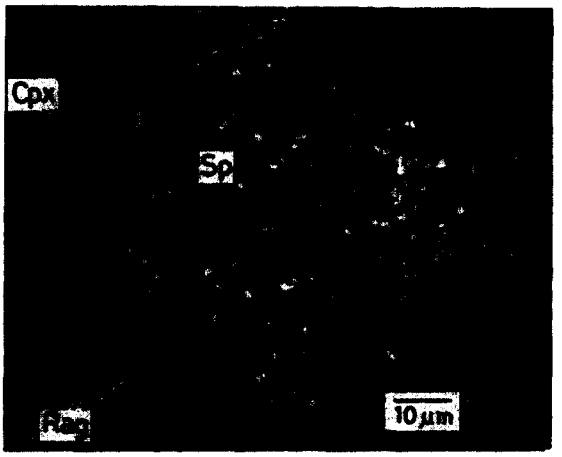

FIG. 10. BSE image of 55115, a heavily altered inclusion, showing its spinel-rich core embayed and veined by ilmenite (bright)-bearing ragged material which also encloses the entire core and is enclosed, in turn, by a very thin, discontinuous clinopyroxene rim. Abbreviations as used previously.

Matrix

As seen around the Al-rich inclusion in Fig. 7 and the cluster in Fig. 9, the matrix of amoeboid olivine aggregates is composed predominantly of poorly-sorted (<1–40 μm) olivine grains. Some of the largest grains are angular to subrounded, polycrystalline aggregates in which individual olivine crystals are zoned from FeO-poor cores to FeO-rich rims. These are strikingly similar to olivine grains comprising nearby olivine clumps (Fig. 7), as are smaller, angular, FeO-rich, unzoned olivine grains in the matrix (Fig. 7, left). The matrix contains lesser amounts of feldspathoids (Fig. 9, dark) as angular grains reaching 30 μm in length and often enclosing elongated olivine. Lumps containing the hedenbergite-rich assemblage (Fig. 9, bright) are common, metallic nickel-iron ($\sim Ni_{66}Fe_{34}$) and pentlandite minor and calcium phosphate and chromite-rich spinel rare constituents of the matrix. All of these angular matrix constituents also occur as parts of olivine clumps or attached to them, suggesting that the matrix of amoeboid olivine aggregates could have formed, at least in part, by fragmentation of olivine clumps. Indeed, the textural similarity and proximity of angular, polycrystalline olivine clasts to olivine inside clumps suggests that the former are pieces broken and removed a short distance away from the latter.

As pointed out by BAR-MATTHEWS *et al.* (1979), however, there is another textural component in the matrix of amoeboid olivine aggregates. It consists of relatively well-sorted, loosely-packed, randomly-oriented plates of relatively FeO-rich olivine mixed with lesser interstitial feldspathoids. These plates are elongated, reach 5–15 μm in length and resemble those comprising the matrix of Allende and Layer III of accretionary rims around coarse-grained Allende inclusions in both morphology and composition. This type of matrix is seen at the top of Fig. 7, adjacent to the poorly-sorted matrix.

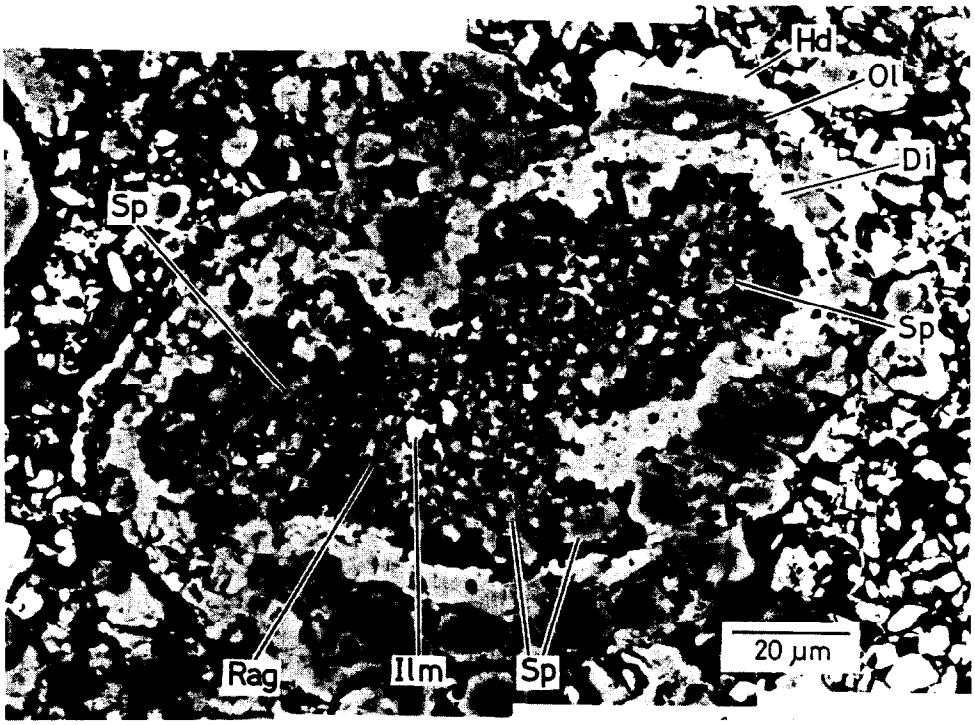

FIG. 11. BSE image of 55111, a very heavily altered inclusion, showing porous core made mostly of ragged material, highly irregular spinel grains and ilmenite. Abbreviations as used previously.

MINERAL CHEMISTRY

Primary minerals

Melilite. Melilite occurs only in the cores of the lightly altered inclusions 55101 and 55102. Analyses are shown in Table 1. In 55101, it ranges in composition from Ge 85 to Ge 96, with an average of Ge 92, and in 55102, from Ge 92 to Ge 98, with an average of Ge 95. KORNACKI and WOOD (1985) showed that gehlenitic melilite is characteristic of spinel-rich objects in Allende, including those inside amoeboid olivine aggregates. Gehlenitic melilite is also characteristic of fluffy Type A, Ca-, Al-rich inclusions (ALLEN *et al.*, 1978; MACPHERSON and GROSSMAN, 1984) and some refractory inclusions in Murchison, the BB and MUM inclusions of MACPHERSON *et al.* (1983).

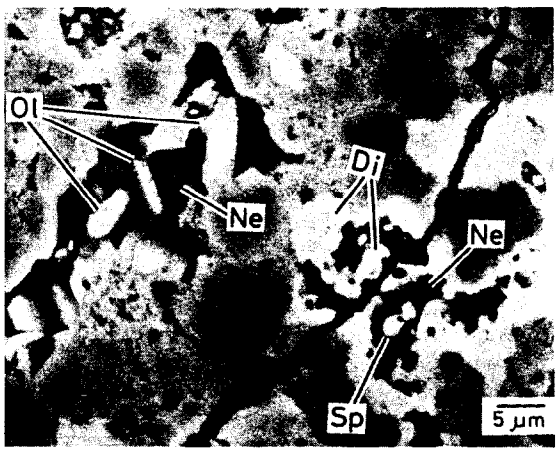

FIG. 12. BSE image of 51113-1, a very heavily altered inclusion (upper left), and 51113-2, a moderately altered one (lower right) inside the same olivine clump. Olivine-feldspathoid inclusions like 51113-1 are very abundant. Note the euhedral olivine in 51113-1 and the aluminous diopside rim around 51113-2, separating it from the surrounding, massive olivine. Abbreviations as used previously.

Melilite in 55101 and 55102 is either very fine-grained (<2 μm) with a distinct chemical composition from one grain to another, or is coarser and chemically zoned, judging from analyses within 1–2 μm of each other which often show significantly different compositions from each other, *e.g.* Ge 88 and Ge 94.

The melilite also contains, in wt%, <.01–.22 (.06 on average) Na_2O, <.01–.03 (.01) K_2O, <.03 Sc_2O_3, <.04–.41 (.12) TiO_2, <.02–.03 (<.02) V_2O_3, <.03–.06 (<.03) Cr_2O_3, <.02–.08 (<.02) MnO and .03–.19 (.09) FeO.

The Na_2O and FeO contents of melilite increase from the centers to the edges of the cores of these inclusions, as shown in Fig. 13. Together with the presence of feldspathoids as alteration products in these inclusions and the observation that spinel in the mantles is richer in FeO than that in the cores, this suggests that Na_2O and FeO were introduced into melilite during alteration. No systematic differences in MgO and TiO_2 contents were seen from center to edge.

Clinopyroxene. Fassaite occurs in the interiors of lightly altered and moderately altered inclusions, and

Table 1. Electron microprobe analyses of primary phases in Al-rich inclusions in amoeboid olivine aggregates

	Mel	Mel	Mel	Mel	Sp	Sp	Sp	Pv
Na_2O	0.08	0.04	0.17	0.01	<0.01	0.01	0.02	<0.01
MgO	0.82	0.64	1.21	0.85	27.80	22.86	26.56	0.06
Al_2O_3	34.98	35.73	33.83	34.77	70.92	68.40	70.03	0.25
SiO_2	23.21	22.98	24.10	22.38	0.04	0.05	0.07	0.03
K_2O	0.02	0.01	<0.01	0.02	0.02	0.03	0.02	0.02
CaO	40.06	41.18	40.52	39.94	0.07	0.13	0.12	40.04
Sc_2O_3	<0.03	<0.03	<0.03	<0.03	<0.03	<0.03	<0.03	0.03
TiO_2	0.41	0.18	<0.04	0.12	0.26	0.33	0.06	56.78
V_2O_3	0.02	0.03	<0.02	<0.02	0.11	0.14	0.13	0.05
Cr_2O_3	<0.03	<0.03	<0.03	<0.03	0.11	0.23	0.20	<0.03
MnO	<0.02	0.04	<0.02	0.02	<0.02	0.04	0.05	0.02
FeO	0.13	0.10	0.16	0.08	0.63	7.91	2.75	0.09
Total:	99.73	100.93	99.99	98.19	99.96	100.13	100.01	97.37
	Cations per 14 Oxygen Ions				Cations per 24 Oxygen Ions			
Na	0.014	0.007	0.030	---	---	0.003	0.005	---
Mg	0.111	0.086	0.164	0.118	5.913	5.022	5.706	0.017
Al	3.766	3.812	3.634	3.809	11.926	11.881	11.896	0.055
Si	2.120	2.080	2.197	2.080	0.006	0.007	0.010	0.006
K	0.002	0.001	---	0.002	0.003	0.005	0.003	0.004
Ca	3.921	3.993	3.957	3.978	0.010	0.020	0.018	7.976
Sc	---	---	---	---	---	---	---	0.006
Ti	0.028	0.013	---	0.008	0.028	0.036	0.007	7.938
V	0.002	0.002	---	---	0.013	0.017	0.015	0.008
Cr	---	---	---	---	0.012	0.027	0.023	---
Mn	---	0.003	---	0.002	---	0.005	0.006	0.003
Fe	0.010	0.008	0.012	0.006	0.075	0.975	0.332	0.015
Total:	9.974	10.005	9.994	10.003	17.986	17.998	18.021	16.028

Mel = melilite
Sp = spinel
Pv = perovskite

also constitutes the inner layer of the clinopyroxene rim of these inclusions. Aluminous diopside constitutes the outer rim layer in most Al-rich inclusions.

Representative analyses are shown in Table 2. The pyroxene composition range is larger than that reported by GROSSMAN (1975) for pyroxene from Allende coarse-grained inclusions. As in the latter inclusions, cation sums for pyroxene in this study are systematically below 16 on the basis of 24 oxygen atoms when all Ti is calculated as TiO_2, and become progressively smaller with increasing Ti content. These data suggest that 40–70% of the total Ti in the pyroxene of amoeboid olivine aggregates is trivalent, as in the case of coarse-grained inclusions.

Clinopyroxene also contains, in wt%, <.01–.07 (.02 on average) Na_2O, <.01–.05 (.02) K_2O, <.03–.60 (.06) Sc_2O_3, <.02–.44 (.21) V_2O_3, <.03–.11 (.04) Cr_2O_3, <.02–.08 (.03) MnO and <.02–.74 (.27) FeO. V concentrations correlate positively with those of Al and Ti.

The clinopyroxene grains with the lowest FeO concentrations, <.02–.10 wt%, are those in the cores of lightly altered inclusions. In these inclusions, clinopyroxene in the mantles and rims contains more FeO than that in the cores. No systematic difference in FeO content of clinopyroxene was seen between the cores and rims of moderately altered inclusions.

Spinel. Spinel occurs as a major phase in lightly, moderately and heavily altered Al-rich inclusions but as a minor, relict phase in very heavily altered ones. Representative analyses are given in Table 1. It is usually close to pure $MgAl_2O_4$. The FeO content ranges from .07 to 12.10 wt%, the average of 63 analyses being 3.96 wt%. As shown in Fig. 14, the FeO contents of spinel grains increase substantially from the interiors to the exteriors of lightly and moderately altered inclusions and the average FeO content of spinel increases generally from lightly to heavily and very heavily altered types.

The spinel in lightly, moderately and heavily altered inclusions also contains, in wt%, <.01–.03 (.01 on average) Na_2O, <.01–.87 (.15) SiO_2, <.01–.03 (.02) K_2O, .02–.57 (.15) CaO, <.03–.06 (.03) Sc_2O_3, <.04–.79 (.29) TiO_2, <.02–.75 (.23) V_2O_3, <.03–.93 (.21) Cr_2O_3 and <.02–.09 (.03) MnO. Although the FeO content does not correlate with the content of SiO_2, CaO, TiO_2 or V_2O_3, there is a positive, but poor, correlation between FeO and Cr_2O_3 as observed by KORNACKI and WOOD (1985) in their Type 1B inclusions. Spinel in very heavily altered inclusions is richer in Cr_2O_3, >0.9 wt%,

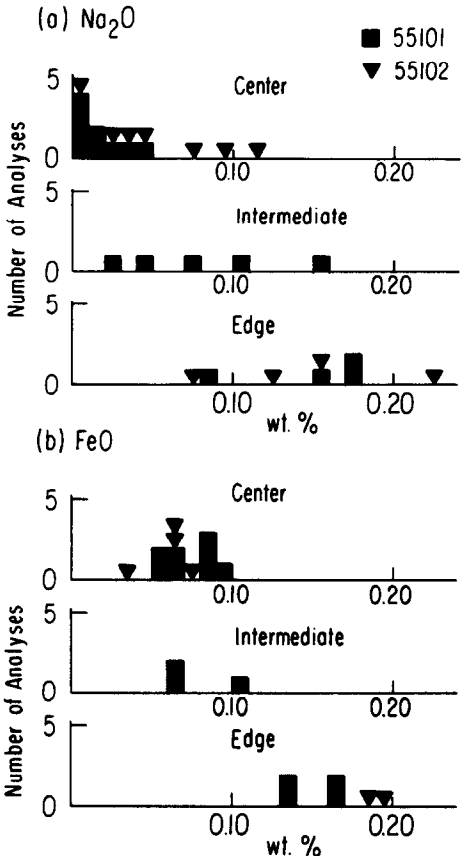

FIG. 13. (a) Na_2O and (b) FeO contents of melilite in the centers, edges and regions intermediate between these locations in the cores of 55101 and 55102.

than, poorer in CaO, <0.2 wt%, than and similar in TiO_2 to that in less altered inclusions. Some spinel analyses in the former inclusions are high in SiO_2, >1.0 wt%, but this may be due to contamination by surrounding olivine.

Perovskite. Because of its scarcity and small grain size, only three analyses of perovskite were obtained, one of which is given in Table 1. Perovskite in the central cores of 55101 and 55102 is nearly pure $CaTiO_3$ with <0.1 wt% of every other oxide except Al_2O_3. One of these grains near the mantle of 55102 shows extreme iron enrichment in its rim.

Secondary minerals

Grossular and anorthite. These phases coexist in lightly and moderately altered inclusions. Two analyses of each are shown in Table 3.

Nine analyses of grossular showed, in wt%, .88–3.63 (2.22 on average) Fe, .67–1.82 (1.24) MgO and .10–.53 (.23) MnO. Although the analyses in Table 3 assume that Fe is divalent, the stoichiometry of calculated chemical formulae is improved if Fe is assumed to be trivalent. The grossular also contains <.01–.17 (.06) Na_2O, <.01–.03 (<.01) K_2O, <.03–.07 (<.03) Sc_2O_3, <.04–.28 (.11) TiO_2, <.02–.05 (<.02) V_2O_3 and <.03–.07 (.03) Cr_2O_3.

Ten analyses of anorthite showed, in wt%, <.01–.59 (.20 on average) Na_2O and .11–1.16 (.50) MgO. There is so little Na that it cannot be determined whether it exists as albite molecule or whether it is due to slight contamination by adjacent nepheline. The MgO contents reported here are very high for anorthite, even compared to the unusually high values, .005–.13 wt%, obtained from high precision analyses of anorthite in Allende Type B inclusions by HUTCHEON *et al.* (1978). For this reason, contamination of the present analyses by spinel and/or clinopyroxene is suspected, although agreement with anorthite stoichiometry is no poorer for analyses with high MgO than for those with low MgO. The anorthite also contains <.01–.04 (.02) K_2O, <.03–.04 (<.03) Sc_2O_3, <.04–.06 (<.04) TiO_2, <.02 V_2O_3, <.03 Cr_2O_3, <.02–.05 (.02) MnO and .03–.28 (.16) FeO. There appear to be crude, positive correlations between Na, Mg and Fe concentrations.

Nepheline. As discussed above, nepheline in lightly, moderately and heavily altered inclusions is an alteration product of anorthite which, in turn, was derived from melilite. In very heavily altered inclusions, nepheline is also an alteration product of spinel and clinopyroxene. Matrix nepheline appears to be closely related to that in very heavily altered inclusions, as both frequently contain elongated olivine crystals.

Representative analyses are shown in Table 3. Thirty-six electron probe analyses of nepheline from all of the above occurrences show, in wt%, 1.46–2.19 (1.80 on average) K_2O and 1.23–2.27 (1.72) CaO, similar to values previously reported for nepheline in amoeboid olivine aggregates (GROSSMAN and STEELE, 1976). Nepheline also contains <.01–.47 (.06) MgO, <.03–.06 (<.03) Sc_2O_3, <.04–.08 (<.04) TiO_2, <.02 V_2O_3, <.03–.08 (.05)Cr_2O_3, <.02–.45 (.03) MnO and <.02–.95 (.27) FeO. K/Na and Ca/Na ratios vary from grain to grain. The atomic Ca/Na ratios decrease from ~.70 for grains in lightly altered inclusions to ~.50 for those in very heavily altered inclusions and in the matrix.

The ragged material. This material occurs in all alteration types of Al-rich inclusions and in the matrix of amoeboid olivine aggregates. X-ray diffraction patterns were made of samples excavated from those regions of amoeboid olivine aggregates TS55F1 and TS43F1 known to contain Al-rich inclusions that contain relatively large amounts of ragged material. Aside from diffraction lines from olivine, diopside, nepheline, sodalite and spinel, several weak lines of at least one additional phase are present: 10.1, 7.3, 5.4, 4.75, 4.51, 3.99, 2.93 and 2.67 Å for the former and 10.2, 8.6, 7.8, 4.59 and 2.68 Å for the latter. The ~10 Å spacing is characteristic of mica and the ~7 Å spacing is characteristic of a serpentine or clay mineral. The X-ray data thus suggest the presence of two phyllosilicates in the ragged material. As a further test for the presence of phyllosilicates, an AEI IM20 ion microprobe with

Table 2. Electron microprobe analyses of pyroxene in Al-rich inclusions in amoeboid olivine aggregates

	Int	Int	Int	Rim	Rim	Di	Di
Na_2O	<0.01	<0.01	0.03	<0.01	0.03	0.04	0.06
MgO	3.25	7.28	9.19	8.78	9.61	16.26	15.98
Al_2O_3	27.08	23.08	19.69	19.26	19.98	7.43	6.89
SiO_2	21.92	32.67	37.38	36.12	37.02	50.06	49.07
K_2O	0.03	<0.01	0.01	0.03	0.01	0.02	0.04
CaO	23.68	24.62	24.94	24.94	24.46	25.27	25.08
Sc_2O_3	0.60	0.03	0.05	0.07	0.06	<0.03	<0.03
TiO_2	22.22	11.60	7.90	9.88	7.80	0.13	0.95
V_2O_3	0.30	0.44	0.38	0.19	0.20	0.07	0.03
Cr_2O_3	<0.03	0.08	0.03	0.06	0.03	0.04	0.05
MnO	<0.02	0.02	<0.02	<0.02	0.02	<0.02	<0.02
FeO	0.10	0.23	0.34	0.13	0.18	0.51	0.39
Total:	99.18	100.05	99.94	99.46	99.40	99.83	98.54
			Cations per 24 Oxygen Ions				
Na	---	---	0.009	---	0.009	0.011	0.017
Mg	0.742	1.612	2.020	1.945	2.120	3.518	3.510
Al	4.892	4.040	3.422	3.374	3.485	1.271	1.197
Si	3.359	4.852	5.512	5.368	5.478	7.265	7.230
K	0.005	---	0.002	0.005	0.002	0.003	0.007
Ca	3.889	3.917	3.940	3.971	3.878	3.930	3.959
Sc	0.080	0.004	0.006	0.009	0.008	---	---
Ti	2.561	1.296	0.876	1.105	0.868	0.014	0.105
V	0.037	0.053	0.045	0.022	0.024	0.008	0.004
Cr	---	0.010	0.004	0.007	0.004	0.004	0.006
Mn	---	0.003	---	---	0.003	---	---
Fe	0.013	0.029	0.042	0.016	0.022	0.062	0.048
Total:	15.578	15.816	15.878	15.822	15.901	16.086	16.083

Int = interior fassaite
Rim = rim fassaite
Di = aluminous diopside

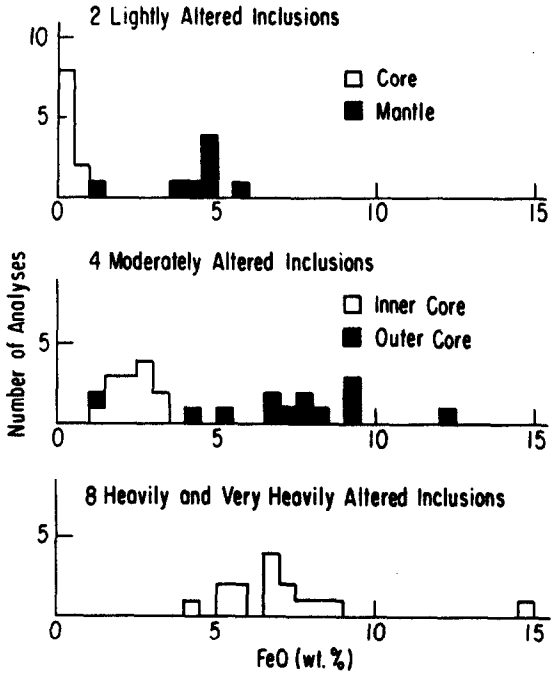

FIG. 14. FeO contents of spinel in various locations inside Al-rich inclusions.

an ~5 μA primary beam of $^{16}O^-$ ions was used to determine directly the abundance of H_2O in patches of the ragged material in very heavily altered inclusions. The instrument was operated at 20 keV and $M/\Delta M$ ~ 300. One per cent H_2O was found. This is more than ten times the signal obtained from fine-grained, olivine-rich areas in Allende thin sections. The amount of H_2O found is a very approximate value for two reasons. Because the ~10 μm beam diameter is larger than the patches of ragged material, the analytical volumes contain some of the surrounding clinopyroxene, making the H_2O determination only a lower limit to the H_2O content of the ragged material. Also, ion yields may be significantly different in the phases in the ragged material from those in the amphibole used as a water standard. Nevertheless, water is definitely present, supporting the identification of the phases in the ragged material as phyllosilicates.

Twenty-three spot analyses of the ragged material were obtained with the SEM and twenty-four by electron microprobe. Examples of the latter are given in Table 4. The ragged material is rich in MgO, Al_2O_3 and SiO_2, always contains ≥1 wt% of each of Na_2O and K_2O and has highly variable FeO and TiO_2 contents. The latter feature is probably due to variable

Table 3. Electron microprobe analyses of secondary phases in Al-rich inclusions in amoeboid olivine aggregates

	An	An	Gr	Gr	Ne	Ne	Ol	Ol	Hd	Hd
Na_2O	0.05	0.24	<0.01	0.07	17.70	17.70	0.02	0.05	0.02	<0.01
MgO	0.36	0.69	0.67	1.74	0.01	0.01	50.11	49.87	0.13	1.11
Al_2O_3	36.63	35.97	20.88	22.49	35.48	35.83	1.71	0.99	0.07	0.09
SiO_2	41.79	40.54	39.07	38.10	43.72	43.16	39.97	40.65	47.66	48.35
K_2O	<0.01	0.04	<0.01	0.01	1.85	1.81	0.02	0.03	0.02	0.02
CaO	19.64	18.36	34.97	33.79	1.56	1.73	0.22	0.16	23.22	23.04
Sc_2O_3	n.a.	0.04	n.a.	n.a.	<0.03	<0.03	<0.03	<0.03	<0.03	<0.03
TiO_2	<0.04	<0.04	0.05	0.14	<0.04	<0.04	<0.04	0.05	<0.04	<0.04
V_2O_3	n.a.	<0.02	n.a.	n.a.	n.a.	n.a.	<0.02	0.02	<0.02	<0.02
Cr_2O_3	<0.03	0.03	<0.03	0.06	<0.03	<0.03	0.03	<0.03	<0.03	<0.03
MnO	0.05	<0.02	0.11	0.11	<0.02	0.06	0.10	0.06	0.15	0.14
FeO	0.03	0.18	2.63	1.13	0.34	0.19	8.33	8.15	27.25	26.63
Total:	98.55	96.09	98.38	97.64	100.66	100.49	100.51	100.03	98.52	99.38
					Cations per 24 Oxygen Ions					
Na	0.012	0.067	---	0.020	4.832	4.842	0.005	0.014	0.006	---
Mg	0.076	0.149	0.154	0.399	0.002	0.002	10.860	10.840	0.032	0.272
Al	6.092	6.134	3.788	4.074	5.887	5.958	0.293	0.170	0.014	0.018
Si	5.898	5.866	6.015	5.855	6.155	6.089	5.811	5.927	7.971	7.967
K	---	0.007	---	0.003	0.332	0.326	0.003	0.005	0.004	0.004
Ca	2.969	2.846	5.768	5.564	0.235	0.261	0.034	0.025	4.162	4.068
Sc	---	0.005	---	---	---	---	---	---	---	---
Ti	---	---	0.006	0.016	---	---	---	0.005	---	---
V	---	---	---	---	---	---	---	0.003	---	---
Cr	---	0.003	---	0.008	---	---	0.003	---	---	---
Mn	0.006	---	0.014	0.014	---	0.007	0.012	0.007	0.020	0.018
Fe	0.004	0.022	0.339	0.145	0.040	0.022	1.013	0.994	3.812	3.670
Total:	15.057	15.099	16.084	16.098	17.483	17.507	18.034	17.990	16.021	16.017

n.a. - not analyzed
An - anorthite
Gr - grossular
Ne - nepheline
Ol - olivine
Hd - hedenbergite

amounts of finely disseminated ilmenite in the ragged material. Before deriving chemical formulae for the ragged material, the maximum possible contribution of ilmenite to the FeO and TiO_2 contents was subtracted from each analysis. As a result of this process, which led to the subtraction of 0.25–4.5% ilmenite in most cases, most of the formulae contain no Ti. Prior to subtraction of ilmenite, analytical sums ranged from 74 to 97% and averaged 88%. The low totals are partly due to the presence of H_2O and partly to the high porosity of the analysed patches of ragged material.

In the absence of accurate water determinations, chemical formulae were calculated from the anhydrous parts of the analyses of the ragged material on the basis of 22 oxygen atoms in order to see if analyses of this material correspond to those of a mica. Figure 15 is a plot of the number of Al cations *vs.* the number of Si cations calculated in this way. Also shown is a reference line connecting the compositions of the ideal mica end-members, phlogopite, $K_2Mg_5Si_6Al_2O_{20}(OH)_4$, and eastonite, $K_2Mg_5AlSi_5Al_3O_{20}(OH)_4$. Most data points from this study lie close to this line, in a cluster stretched out along its length. This indicates that the ragged material may be composed largely of a mica in this solid solution series, although other phyllosilicates also exhibit this behavior. A sufficient number of Al cations was added to the number of Si cations to yield a total of 8 tetrahedral cations and the remaining Al was assigned to octahedral sites. All K, Na and Ca cations were assigned to the interlayer sites and the sum of the interlayer cations was plotted against the sum of the octahedral cations in Fig. 16. The composition field of micas is also shown, extending from theoretical upper limits of 2.0 interlayer and 6.0 octahedral cations to lower limits observed in metamorphic rocks (GUIDOTTI, 1984) of 1.65 interlayer and 5.6 octahedral cations. It is seen that, by these criteria, only 20 of the 47 data points have chemical formulae within error of those for micas. With a mean atomic Fe/Mg ratio of 0.035, the phase represented by these analyses would be termed a phlogopite except for the very high atomic Na/K ratios, ranging from 0.93 to 6.34 and averaging 2.9 ± 1.6. Although CARMAN (1974) synthesized a pure sodium phlogopite at high

Table 4. Electron microprobe analyses of the ragged phyllosilicate in Al-rich inclusions in amoeboid olivine aggregates

SAMPLE	37	45	46	50	30	54
Na_2O	3.46	3.70	3.91	3.17	3.31	3.18
MgO	20.53	20.31	23.10	28.36	23.17	21.24
Al_2O_3	19.86	20.17	18.33	13.82	21.56	25.81
SiO_2	34.37	32.79	36.15	39.57	32.93	32.23
K_2O	2.34	1.32	2.74	3.29	2.16	1.64
CaO	2.53	2.39	1.69	1.26	0.61	0.66
Sc_2O_3	0.12	<0.03	<0.03	0.07	<0.03	<0.03
TiO_2	=0.00	=0.00	=0.00	=0.00	<0.04	=0.00
V_2O_3	<0.02	<0.02	<0.02	<0.02	<0.02	<0.02
Cr_2O_3	<0.03	0.47	<0.03	<0.03	<0.03	0.71
MnO	<0.02	<0.02	<0.02	<0.02	<0.02	0.07
FeO	0.76	0.96	0.85	1.99	2.16	2.79
Subtotal	83.97	82.11	86.77	91.53	85.90	88.33
Ilmenite	6.34	4.06	3.29	3.63	0.00	1.67
Total	90.31	86.17	90.06	95.16	85.90	90.00
Mica:	100%	100%	100%	76.2%	64.7%	55.1%
Si	5.29	5.16	5.40	5.65	4.98	4.73
Al	2.71	2.84	2.60	2.35	3.02	3.27
Total Tet	8.00	8.00	8.00	8.00	8.00	8.00
Al	0.90	0.90	0.63	0.11	0.89	1.03
Mg	4.72	4.76	5.15	5.66	4.86	4.55
Sc	0.02	0.00	0.00	0.01	0.00	0.00
Ti	0.00	0.00	0.00	0.00	0.00	0.00
V	0.00	0.00	0.00	0.00	0.00	0.00
Cr	0.00	0.06	0.00	0.00	0.00	0.08
Mn	0.00	0.00	0.00	0.00	0.00	0.01
Fe	0.10	0.13	0.11	0.22	0.25	0.33
Total Oct	5.74	5.85	5.89	6.00	6.00	6.00
Na	1.03	1.13	1.13	1.05	1.31	1.38
K	0.46	0.26	0.52	0.72	0.56	0.47
Ca	0.42	0.40	0.27	0.23	0.13	0.16
Total Int	1.91	1.79	1.92	2.00	2.00	2.01
Chlorite:	=0%	=0%	=0%	23.8%	35.3%	44.9%
Si				1.80	1.58	1.51
Al				0.20	0.42	0.49
Total Tet				2.00	2.00	2.00
Al				0.31	0.74	1.03
Mg				2.53	2.00	1.54
Sc				0.00	0.00	0.00
Ti				0.00	0.00	0.00
V				0.00	0.00	0.00
Cr				0.00	0.00	0.03
Mn				0.00	0.00	0.00
Fe				0.10	0.10	0.11
Total Oct				2.94	2.84	2.71

temperatures, this phase hydrates at room temperature, losing its 10 Å *d*-spacing. SCHREYER *et al.* (1980) reported terrestrial sodium phlogopite with Na/K ratios from 7 to 30. Those workers reported no X-ray data but their analytical totals are consistent with one of CARMAN's (1974) low-temperature hydration products. Perhaps the phase reported here is a Na-rich phlogopite which, unlike either CARMAN's (1974) phase or the precursor to SCHREYER *et al.*'s (1980) phase, is stable at room temperature because of its greater K_2O content.

The remaining 27 data points on Fig. 16 lie outside of the mica field. Of these, the 8 analyses whose Na + K + Ca > 2.1 may be affected by contamination with intergrown clinopyroxene, as their CaO contents, 0.91–3.69% (average 1.89 ± 0.85%) tend to be higher than those of the other analyses, 0.20–2.84% (average 1.11 ± 0.65%). Eighteen of the data points on Fig. 16 have calculated sums of octahedral cations between 6.1 and 6.46 and total Na + K + Ca between 1.05 and 1.72. These cannot represent mica analyses, but the way in which these and the mica points form a nearly

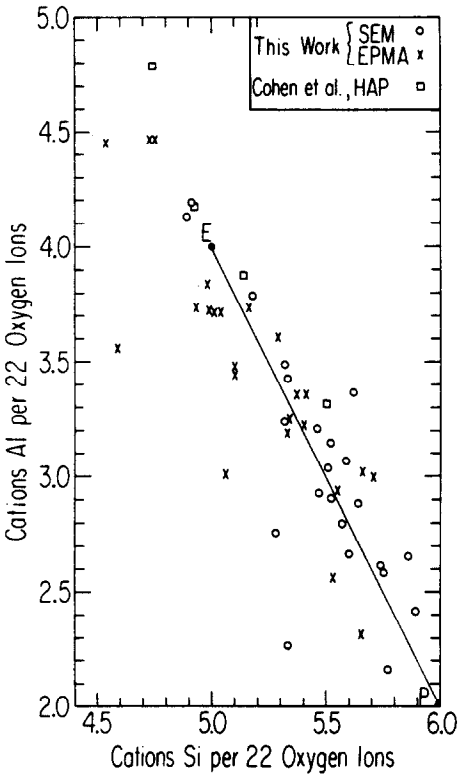

FIG. 15. The number of cations of Al *vs.* the number of cations of Si per 22 oxygen ions in the ragged phyllosilicate. The line connects the ideal compositions of the mica end-members, eastonite (E) and phlogopite (P).

continuous, linear band on this figure suggests that the former points may represent mixtures of mica and a second phase. The second phase may be the additional phyllosilicate indicated by X-ray diffraction. The fact that the material whose analyses yield the latter points is texturally indistinguishable from that yielding the former ones could be explained if the second phyllosilicate were interlayered with the mica. Evidence for such a mixture of phyllosilicates in Allende is the mixed layer mica and montmorillonite-like material reported by TOMEOKA and BUSECK (1982) in fine-grained inclusions.

Assuming that the 18 non-mica data points represent analyses of a mixture of sodium phlogopite and another phyllosilicate, the composition and amount of the latter were calculated in the following way. For each point, a trial chemical formula was calculated for the bulk analysis on the basis of 11 oxygen atoms, as in a mica. The cations were then segregated from one another into two separate phases, each with a formula based on 11 oxygen atoms. In both phases, sufficient Al cations were added to the Si cations to fill four tetrahedral sites and the remaining Al was added to all other trivalent and divalent cations except Ca and assigned to octahedral sites. All K, Na and Ca were assigned to the interlayer sites of the mica which was assumed to have exactly one interlayer cation. All divalent cations in excess of the number required to fill 3 octahedral sites were assigned to the unknown phase. Any separation of charge so produced was balanced by exchanging small amounts of Al from one phase with divalent octahedral cations from the other. The formula of the unknown phase was then recalculated on a 7 oxygen basis, as would be done for an analysis of chlorite, $(Mg, Fe, Al)_3(Si, Al)_2O_5(OH)_4$, when the water content is unknown. The relative molecular proportions of these two phases are then calculated from the original bulk analysis corresponding to each of the 18 data points.

These calculations suggest that from 20 to 59% of a second phyllosilicate is present in the microprobe spots from which these 18 analyses came, the average being 35 ± 11%. The stoichiometry of this phase matches that of no known clay mineral but, when all Al in excess of that necessary to fill two tetrahedral sites is assigned to octahedral sites, the stoichiometric similarity of this phase to chlorite and aluminous lizardite (WICKS and PLANT, 1979) is clear: for the 18 analyses treated in this way, the sum of the octahedral cations ranges from 2.56 to 3.11, the average being 2.84 ± 0.14. Some specific examples of the results of these mixing calculations are shown in Table 4. The first three columns show analyses typical of those which fall in the mica field of Fig. 16. The amounts of TiO_2 and FeO listed are those remaining after subtraction of the maximum ilmenite contribution which is also listed. The correspondence of the formulae calculated on the basis of 22 oxygen atoms to sodium phlogopite is clear. Although small amounts of the second phase could be present in these microprobe spots, the amounts were assumed to be zero since the analyses fall in the mica field. The last three columns of Table 4 show analyses that fall outside the mica field. The formulae for the mica and second phyllosilicate into which these analyses can be broken down are also shown, as well as the molecular proportions of these two phases required for mass balance when the end-members are expressed as one formula unit. Although the second phase is labeled

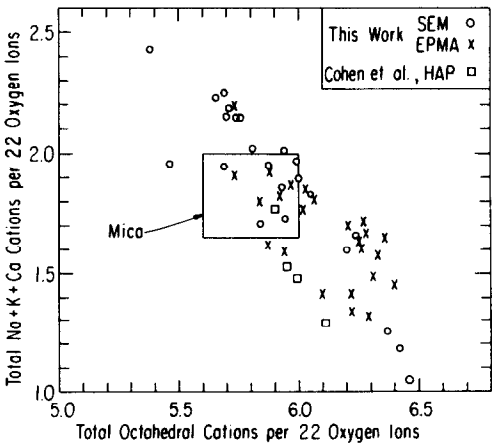

FIG. 16. Total Na + K + Ca cations *vs.* total octahedral cations per 22 oxygen ions in the ragged phyllosilicate. The field of mica is outlined.

chlorite on the table, the observed 7 Å *d*-spacing can be accounted for by either chlorite or aluminous serpentine. Determining which of these phases is actually present would require detailed X-ray study of material relatively free of non-phyllosilicates.

It should be pointed out that decomposition of any one of these bulk analyses does not yield unique compositions for the two components. A mica could have been selected, for example, with specific proportions of cations in the tetrahedral or octahedral site or with total interlayer or octahedral cation sums less than the ideal values. In such cases, the relative amount and composition of the coexisting phase would be different from that calculated above but the stoichiometry of this phase would, in most cases, still be that of a chlorite.

The ragged material is chemically similar to but much lower in Al_2O_3 than the acicular phase observed in the anorthite-, feldspathoid-rich rims on Type A, coarse-grained, Allende inclusions (WARK and LOVERING, 1977) and may be related to the K_2O-rich, layer-structure mineral inferred by DOMINIK *et al.* (1978) to have replaced fassaite in an olivine-rich Allende inclusion. On the basis of HRTEM data showing variable basal fringe spacings between 10 and 15 Å, TOMEOKA and BUSECK (1982) identified phyllosilicate surrounding spinel in an Allende inclusion as a complex mixture of mica and montmorillonite, although no chemical analyses were presented. This could be the ragged material studied here, as the 15 Å line could also be due to chlorite (but not Al-serpentine). COHEN *et al.* (1983) found a high-aluminum phyllosilicate, HAP, in inclusions in the C3 Mokoia. There, it forms the innermost rim layer around spinel, interior to a diopside layer. The similarity in its mode of occurrence to that of the ragged material studied here is parallelled by the similarity in composition between the two phases. The four analyses in that paper were recalculated on a 22 oxygen basis and plotted on Figs. 15 and 16. One data point falls in the mica field, one plots with the two-phase data points of this study and two fall between the two regions. HAP, like the ragged material, may be a mixture of sodium phlogopite and a chlorite or aluminous serpentine in various proportions. Treated in an identical fashion to our analyses, COHEN *et al.*'s (1983) analysis which lies closest to our two-phase mixtures yields 46% chlorite with an octahedral cation sum of 2.55, which is just below the lowest value obtained in this study. Although COHEN *et al.* (1983) claimed that their X-ray diffraction data strongly suggest that HAP is predominantly phyllosilicates, none of the lines at $d > 5$ Å so characteristic of these phases were found by them. They concluded that HAP may be a fine-grained mixture of phases, one of which may be Al-serpentine. FEGLEY and POST (1985) reported a phase with a formula similar to that inferred for HAP near the inner edges of Wark-Lovering rim sequences around spinel in an inclusion in the C3 Kaba. Although no chemical analysis was given, TOMEOKA and BUSECK (1986) reported an approximate chemical formula for Mokoia HAP which is close to those of the two-phase mixtures of this study. They suggested that HAP may be a high-Al saponite and, because of the high alkali content, that the latter is intergrown with mica. Our analyses suggest that, if mica is present, the remaining material consistently has much higher ratios of non-tetrahedral to tetrahedral cations than saponite or any other smectite.

The ragged material contains, in wt%, <.03–.06 (.03 on average) Sc_2O_3, <.02–.42 (.21) V_2O_3, <.03–.71 (.26) Cr_2O_3 and <.02–.07 (.02) MnO.

Olivine. Olivine occurs in the cores of heavily and very heavily altered inclusions and is enclosed by feldspathoids in the latter. It contains substantial iron (Fo 80–92) and is unzoned. Seven electron probe analyses from very heavily altered inclusions show high (0.3–6.0%) Al_2O_3 which cannot be due to nepheline contamination because they also show low Na_2O (<0.4%) and K_2O (<0.1%). Cation sums are close to the ideal value for both olivine and spinel. This, together with the observation of occasional spinel specks within associated feldspathoids, suggests that the high Al_2O_3 may be due to small spinel grains enclosed by or attached to olivine. The olivine also contains, in wt%, .05–.50 (.19 on average) CaO, <.04–.36 (.09) TiO_2, <.02–.20 (.08) MnO, <.03–.05 (<.03) Sc_2O_3, <.02–.03 (<.02) V_2O_3 and <.03–.14 (.05) Cr_2O_3.

Minerals in the hedenbergite-rich assemblage

The results of energy-dispersive analysis of the phases in hedenbergite-rich assemblages in olivine clumps and matrices of amoeboid olivine aggregates and in Wark-Lovering rims and accretionary rims (MACPHERSON *et al.*, 1985) around coarse-grained inclusions are summarized in Table 5. Chemical characteristics common to the phases of this assemblage in all of the above petrographic settings are that hedenbergite and andradite are nearly pure end-members, that wollastonite contains significant FeO but only traces of MgO and that Al_2O_3 contents of hedenbergite and wollastonite are much smaller (~0.5%) than those of diopside and salite (~2%).

Ten electron probe analyses were obtained for hedenbergite. They yield compositions in the range Hd 99–93 Di 1–7. Hedenbergite contains, in wt%, .11–1.11 (.57 on average) MgO, .04–.20 (.09) Al_2O_3, .06–.17 (.13) MnO, <.01–.05 (.02) Na_2O, <.01–.04 (.02) K_2O, <.03–.04 (<.03)Sc_2O_3, <.04 TiO_2, <.02–.07 (<.02) V_2O_3 and <.03–.05 (<.03) Cr_2O_3.

DISCUSSION

Alteration sequence

Table 6 summarizes the mineralogical definitions of the different types of Al-rich inclusions in amoeboid olivine aggregates. Evidence that these inclusions are members of an alteration sequence is not limited to the correlation between the successive disappearance of those phases labeled primary with the successive appearance of those labeled secondary, but also includes the textural interrelationships between primary and secondary phases documented above. Melilite, fassaite, spinel and perovskite are the primary phases

Table 5. Chemical compositions of minerals in hedenbergite-rich assemblages in various petrographic settings by energy-dispersive SEM analysis

Sample	TS55F1	TS51F1	TS43F1	TS58F1	TS24F1	TS34F1	TS10F1	TS10F1
Location	Aoa	Aoa	Aoa	Aoa	W-L	W-L	Ac R	Ac R
Diopside and Salite								
En	43.7	43.5	44.6		45.1	29.9	33.6	30.7
Fs	6.1	4.3	6.4		2.8	17.5	13.8	16.0
Wo	50.2	52.2	49.1		52.1	52.6	52.6	53.3
Al_2O_3 (wt %)	1.7	2.2	1.8		3.6	1.8	<0.1	3.2
No. of analyses	8	2	2		2	2	3	5
Hedenbergite								
En	1.6		0	1.5	0	0	3.0	
Fs	47.2		48.1	45.0	50.0	49.2	45.0	
Wo	51.2		51.9	53.5	50.0	50.8	52.0	
Al_2O_3 (wt %)	<0.1		0.2	0.2	<0.1	0.1	0.1	
No. of analyses	12*		1	1	2	1	8	
Wollastonite								
En					0.4		0.3	
Fs					2.5		8.5	
Wo					97.1		91.2	
Al_2O_3 (wt %)					0.5		<0.1	
No. of analyses					3		2	
Andradite								
And			99.4	99.1			99.6	
Gr			0.6	0.9			0.4	
MgO (wt %)			<0.1	<0.1			<0.1	
Al_2O_3 (wt %)			0.1	0.2			<0.1	
No. of analyses			1	2			2	

* Includes 10 wavelength-dispersive, electron probe analyses
Aoa - inside amoeboid olivine aggregate
W-L - inside Wark-Lovering rim on coarse-grained inclusion
Ac R - inside accretionary rim around coarse-grained inclusion
En - enstatite
Fs - ferrosilite
Wo - wollastonite
And - andradite
Gr - grossular

found in the cores of lightly altered inclusions which contain no secondary phases. In the cores of moderately altered inclusions, melilite is completely altered to grossular and anorthite, and the anorthite, in turn, is partially replaced by feldspathoids. Perovskite is also partially replaced by ilmenite. In heavily altered inclusions, both melilite and fassaite are missing and ragged phyllosilicates and ilmenite have replaced fassaite. In very heavily altered inclusions, all primary phases are absent and spinel has been replaced by either ragged phyllosilicates or olivine and feldspathoids. In the rims of lightly, moderately and heavily altered inclusions, the inner rim layer (fassaite) is partially or completely replaced by ragged phyllosilicates and ilmenite while the outer rim layer (aluminous diopside) is unaltered. This suggests that Al-, Ti-rich clinopyroxene was more susceptible to reaction than Al-, Ti-poor clinopyroxene under the conditions of alteration of Al-rich inclusions.

Table 6. Distribution of minerals in aluminum-rich inclusions in amoeboid olivine aggregates

	Lightly Altered Inclusions	Moderately Altered Inclusions **	Heavily Altered Inclusions	Very Heavily Altered Inclusions
Primary Phases in Core	Melilite	---	---	---
	Fassaite	Fassaite	---	---
	Spinel	Spinel	Spinel	---
	Perovskite	Perovskite	Perovskite †	---
Secondary Phases in Core	---	Anorthite	---	---
	---	Grossular	---	---
	---	Feldspathoids	Feldspathoids	Feldspathoids
	---	---	Ragged Phase	Ragged Phase
	---	---	Olivine †	Olivine
	---	Ilmenite	Ilmenite	Ilmenite
Phases in Inner Rim	Fassaite + Ragged Phase + Ilmenite	Fassaite + Ragged Phase + Ilmenite	Ragged Phase + Ilmenite	Diopside †, *
Phases in Outer Rim	Diopside	Diopside	Diopside	

† Absent in some cases
* Only one layer is recognized as rim.
** Same phases in cores of moderately altered inclusions and mantles of lightly altered ones.

Furthermore, many very heavily altered inclusions retain an aluminous diopside rim, while spinel in their cores is nearly completely altered either to ragged phyllosilicates or olivine + feldspathoids. This indicates that spinel was also more susceptible to reaction than aluminous diopside under these conditions. Even aluminous diopside is replaced by olivine and feldspathoids in very heavily altered inclusions which are relatively small. On this basis, the resistance of primary phases in Al-rich inclusions in amoeboid olivine aggregates to the secondary alteration process which has affected these objects increases in the order melilite, perovskite, fassaite, spinel, aluminous diopside.

MACPHERSON *et al.* (1981) gave strong evidence that clinopyroxene rims on coarse-grained inclusions resulted from alteration of melilite in the interiors of those inclusions. Although clinopyroxene rims on Al-rich inclusions in amoeboid olivine aggregates are very similar to those on coarse-grained inclusions, there is no evidence that the former are alteration products of melilite. Among moderately altered Al-rich inclusions, anorthite, grossular and feldspathoids (the secondary phases derived from melilite) are very minor constituents in the cores of the spinel-rich variety and are much more abundant in the cores of the spinel-poor variety. There is, however, no difference in the thickness of clinopyroxene rims between these two varieties, despite the inferred difference in the amounts of melilite altered in the two varieties.

Chemical fractionations accompanying alteration

In this section, we discuss which elements were gained and lost during each alteration reaction documented above. Aluminum is chosen for normalization as it is a major element in many of the phases involved and because it is very immobile in terrestrial metasomatic processes.

In the alteration of gehlenitic melilite to anorthite and grossular and subsequent alteration of anorthite to nepheline and sodalite, all of the alteration products have higher Si/Al ratios than the starting material, indicating addition of Si during alteration. Relative to melilite, the Ca/Al ratio is lower in anorthite and feldspathoids and higher in grossular. Combined with the observation that the total amount of anorthite and feldspathoids always exceeds that of grossular, this implies that Ca was lost. Examination of Tables 1 and 3 shows that the Ti/Al ratios of anorthite, grossular and nepheline are lower than those of melilite. The Mg/Al ratios of anorthite and nepheline are lower than those of melilite, while those of grossular are slightly higher. Taken together, these data imply that Mg and Ti may have been lost during alteration of melilite. This is not certain, however, as it is not known whether extremely fine-grained, Mg-rich clinopyroxene is present such as that observed by TEM inside anorthite in areas of altered melilite in coarse-grained Allende inclusions (BARBER *et al.*, 1984). Because the melilite in the Al-rich inclusions studied here is so low in MgO and TiO_2, only a small amount of such undetected pyroxene could accommodate the total amounts of these elements that were released during melilite alteration. On average, Na/Al, K/Al and Fe/Al ratios are higher in anorthite and grossular than in melilite, implying introduction of Na_2O, K_2O and FeO during alteration of the latter. This is also indicated by enrichments of Na_2O and FeO in melilite in the outer cores compared to that in the inner cores of lightly altered inclusions (Fig. 13). Addition of SiO_2, Na_2O and FeO also caused alteration of melilite in Allende coarse-grained inclusions (MACPHERSON *et al.*, 1981; WARK, 1981). During alteration of anorthite to feldspathoids in Al-rich inclusions in the present study, it is clear that Na_2O, K_2O and Cl were added and CaO was lost, while the Si/Al ratio remained constant. Nepheline, the predominant feldspathoid, has a much lower Mg/Al ratio than anorthite, suggesting removal of MgO during conversion of anorthite to feldspathoids, again assuming that there are no tiny, undetected pyroxene grains present. During alteration of perovskite to ilmenite, CaO was removed completely and FeO was introduced.

In Fig. 17, chemical compositions of fassaite and the ragged material (after correction for ilmenite) are plotted on the triangular diagram Ca + Mg + Fe-Al-Si. All data points for the ragged material fall in the same region of the diagram as those for fassaite from Al-rich inclusions, providing additional evidence that the ragged material is an alteration product of fassaite. In this diagram, the only difference in composition between the two materials is that the pyroxene points extend to higher and lower Al contents than those for the ragged phyllosilicates. The absence of ragged material with low Al_2O_3 contents is due to the fact that Al-poor clinopyroxene remains unaltered, according to textural evidence mentioned above. The absence of ragged material with Al contents greater than 35 mole% (of the total of the elements plotted in Fig. 17) is probably due to the scarcity of clinopyroxene with such high Al, the only such pyroxene compositions found in this work coming from only two Al-rich inclusions. Despite the fact that the ragged material has very low CaO/MgO ratios compared to fassaite, both materials have a similar range of (Ca + Mg + Fe)/(Al + Si) ratios. This implies that MgO and FeO substitute for CaO during transformation of fassaite to the ragged material. Evidence that FeO was introduced during this process is the much higher Fe/Al ratio of the ragged material (even after subtraction of ilmenite, Table 4) than the starting fassaite (Table 2). Several data points for the ragged material plot outside the pyroxene field in Fig. 17, possibly because of a small amount of nepheline contamination or because of removal of slightly more CaO than the amount of MgO + FeO added during alteration. Na_2O, K_2O and H_2O are also introduced during alteration of fassaite to the ragged material.

Based on the fact that FeO and Cr_2O_3 contents of spinel generally increase with increasing alteration intensity of Al-rich inclusions and with increasing distance from the centers of individual inclusions, these oxides must have been introduced into spinel during

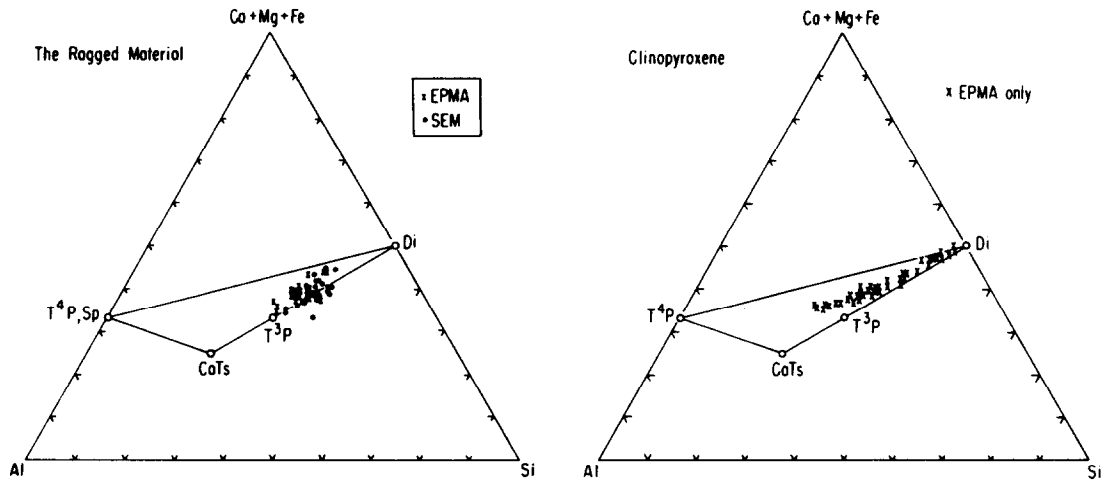

FIG. 17. Comparison of the atomic compositions of primary clinopyroxene and ragged phyllosilicates (after correction for ilmenite) in Al-rich inclusions in amoeboid olivine aggregates. T^4P—$CaTiAl_2O_6$; CaTs—$CaAl_2SiO_6$; T^3P—$CaTiAlSiO_6$; Di—$CaMgSi_2O_6$.

alteration. If Al_2O_3 was immobile during alteration, MgO must have been removed because the MgO/Al_2O_3 ratio of spinel decreases as FeO increases. If spinel alone were altered to the ragged phyllosilicates, addition of SiO_2, MgO, H_2O, alkalis and a small amount of CaO is required to account for the bulk composition of the ragged material. Because CaO was removed in the other alteration reactions, it seems more likely that CaO was provided by clinopyroxene which participated in the spinel alteration reaction than that CaO was introduced from the outside. The relative absence of Al-poor ragged material mentioned above may also be explainable by simultaneous alteration of some Al-poor clinopyroxene and spinel.

It is clear that Na_2O, K_2O and Cl were introduced during alteration of spinel and aluminous diopside to form the olivine and feldspathoids assemblage seen in very heavily altered inclusions. In moderately altered inclusions inside the same olivine lumps as very heavily altered inclusions, aluminous diopside is more abundant than spinel. The spinel and aluminous diopside assemblage thus has a Ca/Al atomic ratio > 0.3 (Tables 1, 2), while that of the feldspathoids which replace it is <0.1, implying loss of CaO in this process.

Conditions of alteration

The anorthite + grossular + feldspathoids that replaced melilite in mantles of lightly altered inclusions and cores of all others in amoeboid olivine aggregates is reminiscent of the secondary alteration product assemblage that formed from melilite in Allende coarse-grained inclusions. Both assemblages may have formed in the same process under similar physico-chemical conditions. GROSSMAN and STEELE (1976) suggested that alteration products in amoeboid olivine aggregates formed by reaction between refractory Ca-, Al-rich minerals and the cooling solar nebular gas and, because feldspathoids occur in the alteration products, proposed that the reactions took place below 900 K. ALLEN *et al.* (1978) argued that alteration of coarse-grained inclusions also resulted from reaction with the solar nebular gas. HUTCHEON and NEWTON (1981) applied thermodynamic calculations to coexisting phases in an Allende Type B inclusion and concluded that alteration of melilite + anorthite to form secondary grossular + monticellite began at 958 K.

Olivine immediately surrounding Al-rich inclusions is usually not in the form of loose aggregates of crystals but rather is massive, suggesting that it nucleated on Al-rich inclusions during condensation instead of accreting around them after condensing elsewhere. Because olivine condenses at a much higher temperature than the formation temperatures of grossular and feldspathoids, the model of GROSSMAN and STEELE (1976) would require alteration of Al-rich inclusions to have occurred after olivine encased the latter, probably by penetration of the altering fluid along cracks and grain boundaries in the olivine mantle. Despite the intense alteration that resulted in formation of phyllosilicates inside Al-rich inclusions, however, olivine surrounding the inclusions has escaped serpentinization completely. The question arises as to how this is possible because the alternative, that olivine condensed around Al-rich inclusions after they were altered, would require very contrived circumstances.

In order to address this question, thermodynamic calculations were performed on the dehydration reactions of serpentine, chlorite and Na-phlogopite to see at what temperature each of these phases would become stable at a solar nebular water fugacity of 10^{-6}. Dehydration reactions resulting in the most stable breakdown products are

$$\underset{\text{antigorite}}{Mg_{48}Si_{34}O_{85}(OH)_{62}} + 20\,\underset{\text{brucite}}{Mg(OH)_2} \rightarrow 34\,\underset{\text{forsterite}}{Mg_2SiO_4} + 51\,H_2O_{(v)} \quad \text{(A)}$$

for serpentine,

$$\underset{\text{clinochlore}}{(Mg_5Al)(Si_3Al)O_{10}(OH)_8} \rightarrow \underset{\text{orthoenstatite}}{Mg_2Si_2O_6} + \underset{\text{spinel}}{MgAl_2O_4} + \underset{\text{forsterite}}{Mg_2SiO_4} + 4H_2O_{(v)} \quad (B)$$

for chlorite, and

$$4\,\underset{\text{Na-phlogopite}}{NaMg_3AlSi_3O_{10}(OH)_2} \rightarrow 6\,\underset{\text{forsterite}}{Mg_2SiO_4} + 3\,\underset{\text{nepheline}}{NaAlSiO_4} + \underset{\text{albite}}{NaAlSi_3O_8} + 4H_2O_{(v)} \quad (C)$$

for Na-phlogopite.

For reactions (A) and (B), for which the standard entropy, ΔS_r^0, and free energy, ΔG_r^0, of reaction can be calculated readily at 298 K and 1 bar pressure, the equilibrium temperature, T, at any other water fugacity, f_{H_2O}, can be calculated from the relation

$$\Delta G_r^0 - (T-298)\Delta S_r^0 + nRT \ln f_{H_2O} = 0 \quad (D)$$

where n is the number of moles of H_2O in the balanced chemical reaction and R is the gas constant, if the volume change of the solid phases in the reaction is ignored and if T is within a few hundred K of 298 K. The assumed f_{H_2O} comes from results of solar nebular condensation calculations at temperatures below those where the sharp increase in P_{H_2O}/P_{H_2} occurs (GROSSMAN, 1972). Using thermodynamic data for antigorite from HELGESON *et al.* (1978) and for all other phases from ROBIE *et al.* (1978), the equilibrium temperature for antigorite is 274 K. Using data from JENKINS and CHERNOSKY (1986), the temperature for clinochlore is 328 K. The maximum possible error for the clinochlore temperature was calculated to be ±26°, a value assumed to be representative of the error on the equilibrium temperature for all three reactions.

For reaction (C), neither the free energy nor the entropy of Na-phlogopite are known at 298 K and 1 bar, so a different approach was used. The equilibrium curve for reaction (C) passes through T = 1113 K and P = 400 bars. The standard free energy of reaction was calculated at this temperature from

$$\Delta G_r^0 = -\Delta V_r^{sol} P - 4RT \ln f_{H_2O}. \quad (E)$$

Using the molar volume for Na-phlogopite from CARMAN (1974) and for all other phases from ROBIE *et al.* (1978), $\Delta G_r^0 = -217345$J. From this, the free energy of reaction, ΔG_r, at $f_{H_2O} = 10^{-6}$ and any temperature can be calculated from

$$\Delta G_r = \Delta G_r^0(1113) - \int_{1113}^{T} \Delta S_r^{0,sol} dT + 4[G_T^{H_2O} - G_{1113}^{H_2O}] + 4RT \ln 10^{-6} \quad (F)$$

where $\Delta S_r^{0,sol}$ is the standard entropy change of the solids in the reaction and $G_{1113}^{H_2O}$ is the free energy of formation of water vapor at 1113 K, if the volume change of the solid phases in the reaction is ignored. The entropy of formation of Na-phlogopite was estimated at several temperatures in the range 400–1000 K in order to calculate $\Delta S_r^{0,sol}$. This was done by assuming that its entropy was the same as that of fluorphlogopite, plus the difference in entropy between $Mg(OH)_2$ and MgF_2, plus the difference in entropy between NaOH and KOH, using data from ROBIE *et al.* (1978). Entropies of formation of all other solid phases and the free energy of water vapor were taken from ROBIE *et al.* (1978) and the free energy of reaction (C) was calculated from (F) over the temperature range 400–800 K. The temperature at which the calculated free energy of reaction at $f_{H_2O} = 10^{-6}$ becomes zero, *i.e.*, the equilibrium temperature, is 470 K.

These calculations suggest that, in the solar nebula, Na-phlogopite would have formed from its most stable dehydration products if the temperature were below 470 K. In Al-rich inclusions in amoeboid olivine aggregates, however, Na-phlogopite formed from fassaite and spinel, an assemblage less stable than forsterite + nepheline + albite + water. This means that the Na-phlogopite reaction could have occurred at $T \geq 470$ K, assuming that the phase relations are unaffected by the K_2O contents of the actual mica observed.

Retrograde alteration of mica to chlorite is a common feature of terrestrial metamorphic rocks. VEBLEN and FERRY (1983) illustrated the results of this process in which layers of biotite unit cells are intergrown with layers of chlorite unit cells in a direction parallel to their c axes. VEBLEN (1983) also showed similar intergrowths of Al-rich chlorite with the Na-mica wonesite, $\sim(Na_{.79}K_{.15})(Mg_{4.39}Fe_{.78}Ti_{.07}Al_{.62})(Al_{1.53}Si_{6.47})O_{20}(OH, F)_4$. It is possible that the ragged material studied here is similarly intergrown Na-phlogopite and Al-rich chlorite and that the chlorite formed from the Na-phlogopite in a similar secondary alteration process. The above calculations show that clinochlore reacts to form its most stable dehydration products at 328 K in a solar gas. Because Na-phlogopite is less stable than the assemblage orthoenstatite + spinel + forsterite + H_2O, however, clinochlore might be expected to form from Na-phlogopite at a slightly higher temperature than this. Assuming that the composition difference between clinochlore and the actual chlorite observed has little effect on the phase relations, secondary alteration of Na-phlogopite to chlorite probably occurred at a temperature ≥328 K, less than the formation temperature of the Na-phlogopite.

Finally, alteration of forsterite in amoeboid olivine aggregates to antigorite + brucite would not have occurred until the temperature of the solar nebular gas fell to 274 K, below the formation temperatures of both Na-phlogopite and chlorite. Thus, it is possible that fassaite and spinel in Al-rich inclusions underwent hydration reactions with the solar nebular gas to form Na-phlogopite and that the latter continued to react to form chlorite without attendant serpentinization of olivine if solids remained in equilibrium with the gas in the temperature range 328–470 K but stopped equilibrating with it before the temperature fell to 274 K. Note that during aqueous alteration in a parent body, a process often invoked to account for phyllosilicates in carbonaceous chondrites (MCSWEEN, 1979), the activity of H_2O would have been high enough to convert both fassaite and forsterite to phyllosilicates.

Clearly, aqueous alteration was not the process whereby fassaite of Al-rich inclusions was hydrated.

Another question is why the atomic Na/K ratio of the meteoritic mica, 0.93–6.34, is so much higher than that of phlogopite-biotite solid solutions found commonly in metamorphosed pelitic rocks on the earth, ≤0.06 (GUIDOTTI, 1984). The answer is probably related to the different bulk compositions of the systems in which these phases originated. Pelitic rocks have the compositions of shales, the average atomic Na/K ratio of which is ~0.6 (TUREKIAN, 1972). If, as is assumed above, the meteoritic phlogopite formed by reaction of Al-rich phases with the solar nebular gas, the alkalis would have been derived from a system of solar composition, in which the atomic Na/K ratio is ~15.1 (ANDERS and EBIHARA, 1982). Thus, the meteoritic mica may have a higher Na/K ratio than its terrestrial counterpart because the system from which the former crystallized had a higher Na/K ratio.

Although melilite was replaced by anorthite + grossular + feldspathoids in mantles of lightly altered inclusions and inner cores of moderately altered ones, fassaite was not replaced by phyllosilicates in these locations. Alteration of fassaite occurred further from the centers of these inclusions, in the rims of lightly altered ones and outer cores of moderately altered ones. Both melilite and fassaite were altered in the cores of heavily and very heavily altered inclusions. This may be related to the greatly different sizes of these objects. Rates of diffusion and gas-solid alteration reactions are much lower at phyllosilicate formation temperatures than at the higher temperatures of grossular formation. This may have resulted in grossular formation at relatively large distances from the gas-solid interfaces of these objects, while phyllosilicate formation may have been restricted to a much narrower zone immediately beneath inclusion surfaces. Because of the relatively small sizes of heavily and very heavily altered inclusions, most fassaite in the latter lies within ~50 μm of their surfaces. Because lightly and moderately altered inclusions tend to be much larger, however, the only fassaite within 50 μm of the surfaces of these inclusions is that in their rims and outer mantles. Spinel may have reacted to form phyllosilicates at an even lower temperature than fassaite, possibly accounting for the persistence of spinel in cores of heavily altered inclusions, despite disappearance of fassaite. Very heavily altered inclusions are so small that both fassaite and spinel are missing from their cores.

KORNACKI and WOOD (1985) suggested that Al-rich inclusions formed by partial distillation of interstellar dust at high temperatures (>1500 K). Because of the significant FeO content of spinel in these inclusions, they argued for distillation in a much more oxidizing gas than one of solar composition, presumably to prevent reduction of FeO in the original interstellar dust. The data presented in this paper show, however, that the FeO content of spinel increases with the degree of low-temperature alteration of its associated phases, both within individual inclusions and from one inclusion to another. This suggests that the FeO content of spinel in these inclusions may have been vanishingly small originally and only increased in a later stage of low-temperature alteration, a situation which does not require a non-solar gas.

CONCLUSION

The primary phases of Al-rich inclusions in amoeboid olivine aggregates underwent alteration reactions with the solar nebular gas. The simplest interpretation of our observations is that, as the temperature fell, melilite was the first primary phase to disappear, being replaced by grossular + anorthite + feldspathoids. Fassaite was the next primary phase to disappear, being replaced by a fine-grained mixture of ilmenite, Na-rich phlogopite and either chlorite or Al-rich serpentine. Spinel was the last phase to be altered, forming either phyllosilicates or a mixture of olivine + feldspathoids. During alteration, SiO_2, Na_2O, K_2O, FeO, Cr_2O_3, H_2O and Cl were introduced from the nebular gas and CaO was lost. MgO may have been lost during the melilite reaction and added during formation of phyllosilicates. Thermodynamic calculations suggest that Na-rich phlogopite could have formed at ~470 K and chlorite at ~328 K at a water fugacity of 10^{-6}, that of a gas of solar composition in this temperature range. The fact that olivine surrounding Al-rich inclusions is not serpentinized indicates cessation of gas-solid equilibrium above 274 K.

Acknowledgements—We are especially thankful to R. C. Newton for assistance with the thermodynamic calculations and to R. H. Hinton for performing the water analyses by ion microprobe. We thank F. C. Bishop for instruction in the use of the Northwestern University electron microprobe. Helpful discussions with S. W. Bailey, J. R. Goldsmith, D. R. M. Pattison and E. Olsen are gratefully acknowledged. This research was supported by the National Aeronautics and Space Administration through grant NAG 9-54.

Editorial handling: S. R. Taylor

REFERENCES

ALLEN J. M., GROSSMAN L., DAVIS A. M. and HUTCHEON I. D. (1978) Mineralogy, textures and mode of formation of a hibonite-bearing Allende inclusion. *Proc. Lunar Planet. Sci. Conf. 9th*, 1209–1233.

ANDERS E. and EBIHARA M. (1982) Solar-system abundances of the elements. *Geochim. Cosmochim. Acta* **46**, 2363–2380.

BARBER D. J., MARTIN P. M. and HUTCHEON I. D. (1984) The microstructure of minerals in coarse-grained Ca-Al-rich inclusions from the Allende meteorite. *Geochim. Cosmochim. Acta* **48**, 769–783.

BAR-MATTHEWS M., MACPHERSON G. J. and GROSSMAN L. (1979) An SEM-petrographic study of amoeboid olivine aggregates in Allende (abstr.). *Meteoritics* **14**, 342.

BENCE A. E. and ALBEE A. L. (1968) Empirical correction factors for the electron microanalysis of silicates and oxides. *J. Geol.* **76**, 382–403.

CARMAN J. H. (1974) Synthetic sodium phlogopite and its two hydrates: Stabilities, properties, and mineralogic implications. *Amer. Mineral.* **59**, 261–273.

COHEN R. E., KORNACKI A. S. and WOOD J. A. (1983) Mineralogy and petrology of chondrules and inclusions in the Mokoia CV3 chondrite. *Geochim. Cosmochim. Acta* **47**, 1739–1757.

DOMINIK B., JESSBERGER E. K., STAUDACHER TH., NAGEL K. and EL GORESY A. (1978) A new type of white inclusion in Allende: Petrography, mineral chemistry, ^{40}Ar-^{39}Ar ages, and genetic implications. *Proc. Lunar Planet. Sci. Conf. 9th*, 1249–1266.

EKAMBARAM V., HASHIMOTO A., DAVIS A. M. and GROSSMAN L. (1985) Trace elements in petrographically-distinct components of Allende inclusions. *Lunar Planet. Sci. XVI*, 205–206.

FEGLEY B. JR. and POST J. E. (1985) A refractory inclusion in the Kaba CV3 chondrite: some implications for the origin of spinel-rich objects in chondrites. *Earth Planet. Sci. Lett.* **75**, 297–310.

GROSSMAN L. (1972) Condensation in the primitive solar nebula. *Geochim. Cosmochim. Acta* **36**, 597–619.

GROSSMAN L. (1975) Petrography and mineral chemistry of Ca-rich inclusions in the Allende meteorite. *Geochim. Cosmochim. Acta* **39**, 433–454.

GROSSMAN L. and STEELE I. M. (1976) Amoeboid olivine aggregates in the Allende meteorite. *Geochim. Cosmochim. Acta* **40**, 149–155.

GROSSMAN L., GANAPATHY R., METHOT R. L. and DAVIS A. M. (1979) Trace elements in the Allende meteorite—IV. Amoeboid olivine aggregates. *Geochim. Cosmochim. Acta* **43**, 817–829.

GROSSMAN L., HASHIMOTO A. and HINTON R. W. (1986) Phyllosilicate inside amoeboid olivine aggregates in Allende (abstr.). *Meteoritics* **21**, 379–380.

GUIDOTTI C. V. (1984) Micas in metamorphic rocks. In *Micas* (ed. S. W. BAILEY), *Reviews in Mineralogy, Vol. 13*, pp. 357–467. Mineralogical Soc. Amer.

HASHIMOTO A. and GROSSMAN L. (1984) Refractory inclusions in amoeboid olivine aggregates in Allende (abstr.). *Meteoritics* **19**, 234–235.

HELGESON H. C., DELANY J. M., NESBITT H. W. and BIRD D. K. (1978) Summary and critique of the thermodynamic properties of rock-forming minerals. *Amer. J. Sci.* **278-A**, 1–229.

HUTCHEON I. D. and NEWTON R. C. (1981) Mg isotopes, mineralogy, and mode of formation of secondary phases in C3 refractory inclusions. *Lunar Planet. Sci. XII*, 491–493.

HUTCHEON I. D., STEELE I. M., SMITH J. V. and CLAYTON R. N. (1978) Ion microprobe, electron microprobe and cathodoluminescence data for Allende inclusions with emphasis on plagioclase chemistry. *Proc. Lunar Planet. Sci. Conf. 9th*, 1345–1368.

JENKINS D. M. and CHERNOSKY J. V. JR. (1986) Phase equilibria and crystallochemical properties of Mg-chlorite. *Amer. Mineral.* **71**, 924–936.

KORNACKI A. S. and FEGLEY B. JR. (1984) Origin of spinel-rich chondrules and inclusions in carbonaceous and ordinary chondrites. *Proc. Lunar Planet. Sci. Conf. 14th; J. Geophys. Res.* **89**(Suppl.), B588–B596.

KORNACKI A. S. and WOOD J. A. (1984a) Petrography and classification of Ca, Al-rich and olivine-rich inclusions in the Allende CV3 chondrite. *Proc. Lunar Planet. Sci. Conf. 14th; J. Geophys. Res.* **89**(Suppl.), B573–B587.

KORNACKI A. S. and WOOD J. A. (1984b) The mineral chemistry and origin of inclusion matrix and meteorite matrix in the Allende CV3 chondrite. *Geochim. Cosmochim. Acta* **48**, 1663–1676.

KORNACKI A. S. and WOOD J. A. (1985) Mineral chemistry and origin of spinel-rich inclusions in the Allende CV3 chondrite. *Geochim. Cosmochim. Acta* **49**, 1219–1237.

MACPHERSON G. J. and GROSSMAN L. (1984) "Fluffy" Type A Ca-, Al-rich inclusions in the Allende meteorite. *Geochim. Cosmochim. Acta* **48**, 29–46.

MACPHERSON G. J., GROSSMAN L., ALLEN J. M. and BECKETT J. R. (1981) Origin of rims on coarse-grained inclusions in the Allende meteorite. *Proc. Lunar Planet. Sci. Conf. 12B*, 1079–1091.

MACPHERSON G. J., BAR-MATTHEWS M., TANAKA T., OLSEN E. and GROSSMAN L. (1983) Refractory inclusions in the Murchison meteorite. *Geochim. Cosmochim. Acta* **47**, 823–839.

MACPHERSON G. J., HASHIMOTO A. and GROSSMAN L. (1985) Accretionary rims on inclusions in the Allende meteorite. *Geochim. Cosmochim. Acta* **49**, 2267–2279.

MCSWEEN H. Y. JR. (1979) Are carbonaceous chondrites primitive or processed? A review. *Revs. Geophys. Space Phys.* **17**, 1059–1078.

ROBIE R. A., HEMINGWAY B. S. and FISHER J. R. (1978) Thermodynamic properties of minerals and related substances at 298.15 K and 1 bar (10^5 pascals) pressure and at higher temperatures. *Geol. Soc. Amer. Bull.* 1452.

SCHREYER W., ABRAHAM K. and KULKE H. (1980) Natural sodium phlogopite coexisting with potassium phlogopite and sodian aluminian talc in a metamorphic evaporite sequence from Derrag, Tell Atlas, Algeria. *Contrib. Mineral. Petrol.* **74**, 223–233.

TOMEOKA K. and BUSECK P. R. (1982) Intergrown mica and montmorillonite in the Allende carbonaceous chondrite. *Nature* **299**, 326–327.

TOMEOKA K. and BUSECK P. R. (1986) Phyllosilicates in the Mokoia CV3 carbonaceous chondrite: petrographic and transmission electron microscope observations. *Lunar Planet. Sci. XVII*, 899–900.

TUREKIAN K. K. (1972) *Chemistry of the Earth.* Holt, Rinehart and Winston.

VEBLEN D. R. (1983) Microstructures and mixed layering in intergrown wonesite, chlorite, talc, biotite, and kaolinite. *Amer. Mineral.* **68**, 566–580.

VEBLEN D. R. and FERRY J. M. (1983) A TEM study of the biotite-chlorite reaction and comparison with petrologic observations. *Amer. Mineral.* **68**, 1160–1168.

WARK D. A. (1981) Alteration and metasomatism of Allende Ca-Al-rich materials. *Lunar Planet. Sci. XII*, 1145–1146.

WARK D. A. and LOVERING J. F. (1977) Marker events in the early evolution of the solar system: Evidence from rims on Ca-Al-rich inclusions in carbonaceous chondrites. *Proc. Lunar Sci. Conf. 8th*, 95–112.

WICKS F. J. and PLANT A. G. (1979) Electron-microprobe and X-ray-microbeam studies of serpentine textures. *Can. Mineral.* **17**, 785–830.